Oncogenic and teratogenic effects of *Trp53*^{Y217C}, an inflammation-prone mouse model of the human hotspot mutant *TP53*^{Y220C}

Sara Jaber[1,7], Eliana Eldawra[1,7], Jeanne Rakotopare[1,7], Iva Simeonova[2], Vincent Lejour[1], Marc Gabriel[3], Tatiana Cañeque[4], Vitalina Volochtchouk[1], Monika Licaj[1], Anne Fajac[1], Raphaël Rodriguez[4], Antonin Morillon[3], Boris Bardot[1,5*], and Franck Toledo[1,6*]

[1]Genetics of Tumor Suppression, Institut Curie, CNRS UMR3244, Sorbonne University, PSL University, Paris, France; [2]Chromatin dynamics, Institut Curie, CNRS UMR3664, Sorbonne University, PSL University, Paris, France; [3]Non Coding RNA, Epigenetic and Genome Fluidity, Institut Curie, CNRS UMR3244, Sorbonne University, PSL University, Paris, France; [4]Chemical Biology, Institut Curie, CNRS UMR3666, INSERM U1143, PSL University, Paris, France; [5]Signaling and Neural Crest Development, Institut Curie, CNRS UMR3347, INSERM U1021, Université Paris-Saclay, PSL University, Orsay, France; [6]Hematopoietic and Leukemic Development, Centre de Recherche Saint-Antoine, INSERM UMRS938, Sorbonne University, Paris, France; [7]These authors contributed equally to this work. *For correspondence: franck.toledo@sorbonne-universite.fr ; boris.bardot@curie.fr.

Abstract

Missense "hotspot" mutations localized in six p53 codons account for 20% of *TP53* mutations in human cancers. Hotspot p53 mutants have lost the tumor suppressive functions of the wildtype protein, but whether and how they may gain additional functions promoting tumorigenesis remain controversial. Here we generated *Trp53*^{Y217C}, a mouse model of the human hotspot mutant *TP53*^{Y220C}. DNA damage responses were lost in *Trp53*$^{Y217C/Y217C}$ cells, and *Trp53*$^{Y217C/Y217C}$ fibroblasts exhibited increased chromosome instability compared to *Trp53*$^{-/-}$ cells. Furthermore, *Trp53*$^{Y217C/Y217C}$ male mice died earlier than *Trp53*$^{-/-}$ males, with more aggressive thymic lymphomas. This correlated with an increased expression of inflammation-related genes in *Trp53*$^{Y217C/Y217C}$ thymic cells compared to *Trp53*$^{-/-}$ cells. Surprisingly, we recovered only one *Trp53*$^{Y217C/Y217C}$ female for 22 *Trp53*$^{Y217C/Y217C}$ males at weaning, a skewed distribution explained by a high frequency of *Trp53*$^{Y217C/Y217C}$ female embryos with exencephaly and the death of most *Trp53*$^{Y217C/Y217C}$ female neonates. Strikingly however, when we treated pregnant females with the anti-inflammatory drug supformin (LCC-12) we observed a five-fold increase in the proportion of viable *Trp53*$^{Y217C/Y217C}$ weaned females in their progeny. Together, these data suggest that the p53^{Y217C} mutation not only abrogates wildtype p53 functions but also promotes inflammation, with oncogenic effects in males and teratogenic effects in females.

Key words

hotspot p53 mutant, p53^{Y220C}, gain of function, exencephaly, inflammation, sex-specific effects.

Introduction

Somatic alterations in the *TP53* gene, encoding the tumor suppressor p53, are the most common events in human tumors (Hollstein et al., 1991). The p53 protein is a stress sensor stabilized and activated in response to potentially oncogenic insults. In its tetrameric active form, wildtype (WT) p53 can trigger a transcriptional program to induce various responses including cell cycle arrest, senescence, apoptosis or metabolic changes (Beckerman and Prives, 2010). In human cancers, about 75% of all *TP53* alterations are missense mutations, and the eight most frequent ("hotspot") missense mutations (R175H, Y220C, G245S, R248Q, R248W, R273H, R273C and R282W) affect six residues localized in the p53 DNA-binding domain (DBD) and account for 20% of all *TP53* mutations (Hainaut and Pfeifer, 2016). The fact that most *TP53* mutations are missense substitutions suggested that cells expressing mutant p53 might have a selective advantage over cells lacking p53, and evidence for this was first gained by expressing various p53 mutants in p53-null cells and observing enhanced tumorigenic potential in nude mice or increased plating efficiency in agar cell culture (Dittmer et al., 1993). Mouse models expressing hotspot p53 mutants next helped to define potential mechanisms accounting for accelerated tumorigenesis. First, a dominant-negative effect (DNE) may be observed in heterozygotes, if the mutant p53 inhibits the WT p53 protein in hetero-tetramers (Gencel-Augusto and Lozano, 2020). Evidence that this mechanism accounts for accelerated tumorigenesis was notably reported in human leukemia (Boettcher et al., 2019). A second mechanism is a gain-of-function (GOF), i.e. the acquisition by mutant p53 of new oncogenic properties (Amelio and Melino, 2020; Stein et al., 2020). Although the DNA sequence specificity of p53 mutants is impaired, leading to a loss of WT functions (LOF), many p53 mutant proteins are stabilized in the cell and might engage in aberrant interactions with other transcription factors, chromatin-modifying complexes or DNA helicase subunits, leading to the acquisition of GOF phenotypes (Kim and Deppert, 2007; Pfister and Prives, 2017; Zhao et al., 2024). However, a few recent studies challenged the pathological importance of mutant p53 GOF, or at least its relevance in anti-cancer therapeutic strategies (Aubrey et al., 2018; Boettcher et al., 2019; Wang et al., 2023). An alternative hypothesis emerged, postulating that the tumorigenic properties of a p53 mutant might result from a separation-of-function (SOF), if the mutant retains pro-proliferative or pro-survival functions of WT p53 while losing its tumor suppressive activities (Kennedy and Lowe, 2022). The concept of SOF was first proposed for *TP53* exon-6 truncating mutations, which mimic a naturally occurring alternative p53

splice variant (Shirole et al., 2016), but may apply to some p53 missense mutations, for example p53^{R248W} (Humpton et al., 2018). Importantly, the analysis of various mutant p53 alleles *in vivo* appears crucial for a better understanding of their contribution to tumorigenesis, because GOF/SOF phenotypes may vary depending on the mutated residue, its specific mutation, the cellular context or genetic background (Dibra et al., 2024; Hanel et al., 2013; Kadosh et al., 2020; Kim and Lozano, 2018; Kotler et al., 2018; McCann et al., 2022; Xiong et al., 2022).

In human cancers, the *TP53*^{Y220C} mutation is the most frequent missense mutation outside of the DNA-binding surface of p53 (Hainaut and Pfeifer, 2016). The somatic *TP53*^{Y220C} mutation accounts for over 100,000 new cancer cases per year worldwide, including solid tumors and myeloid neoplasms, and a germline *TP53*^{Y220C} mutation was reported in 15 families with the Li-Fraumeni syndrome (LFS) of cancer predisposition (Bouaoun et al., 2016; Gener-Ricos et al., 2024). The mutation causes a structural change in the DBD localized at the periphery of the β−sandwich region of the protein, far from the surface contact of DNA. The mutation from a tyrosine to a cysteine markedly lowers the thermodynamic stability of the DBD, leading to a largely unfolded and inactive protein at body temperature (Joerger et al., 2006), and a molecule designed to bind p53^{Y220C} and restore WT protein conformation appears as a promising anti-cancer drug (Dumbrava et al., 2022). Analyses of the impact of p53^{Y220C} in cancer cell lines led to conflicting results. On one hand, overexpression of p53^{Y220C} in a p53-null cell line increased its capacity for migration or invasion (Zhou et al., 2022), and a decreased expression of p53^{Y220C}, caused by RNA interference or various chemical compounds, promoted cell death or decreased the migratory or invasive capacities of cells (Tseng et al., 2022; Vikhanskaya et al., 2007; Zhou et al., 2022). On the other hand, the removal by CRISPR/Cas9 of p53 mutants with reported GOF - including p53^{Y220C} - in diverse cancer cell lines had no significant impact on cell survival or proliferation, and the cell death caused by RNA interference against p53^{Y220C} might result from non-specific toxic effects (Wang et al., 2023). Here, to gain a better understanding of the impact of the p53^{Y220C} mutation *in vivo*, we generated a mouse model with a targeted *Trp53*^{Y217C} mutation - the mouse equivalent to human *TP53*^{Y220C} (Figure S1) - and analyzed animals and cells carrying one or two copies of the mutant allele.

Results

Targeting of a p53^{Y217C} mutation in the mouse

We used homologous recombination in 129/SvJ ES cells to target the p53^{Y217C} mutation at the mouse *Trp53* locus. Mice expressing p53^{Y217C} conditionally were generated by using a targeting vector containing transcriptional stops flanked by LoxP sites (LSL) upstream of coding sequences, and the p53^{Y217C} mutation in exon 6 (Figure 1A-D). *Trp53*$^{+/LSL\text{-}Y217C}$ mice were then crossed with mice carrying the PGK-Cre transgene (Lallemand et al., 1998) to excise the LSL cassette and obtain *Trp53*$^{+/Y217C}$ mice, expressing the mutant protein constitutively. After two backcrosses over a C57BL/6J background, we prepared mouse embryonic fibroblasts (MEFs) from intercrosses of *Trp53*$^{+/Y217C}$ mice (Figure 1E). We extracted RNAs from *Trp53*$^{Y217C/Y217C}$ MEFs then sequenced p53 mRNAs to verify that the p53^{Y217C} coding sequence was identical to the wildtype p53 (p53^{WT}) sequence, except for the desired missense mutation and a silent mutation introduced to facilitate mouse genotyping (Figure 1F). The quantification of p53 mRNA levels from WT and *Trp53*$^{Y217C/Y217C}$ MEFs next revealed similar transcription from both alleles (Figure 1G).

Deficient p53-dependent stress responses in *Trp53*$^{Y217C/Y217C}$ cells

We used western blots to analyze protein extracts from *Trp53*$^{+/+}$, *Trp53*$^{+/-}$, *Trp53*$^{+/Y217C}$, *Trp53*$^{Y217C/Y217C}$ and *Trp53*$^{-/-}$ MEFs, unstressed or treated with Nutlin, an antagonist of Mdm2, the E3 ubiquitin ligase for p53 (Vassilev et al., 2004). Results indicated a high increase in p53 abundance in untreated and Nutlin-treated *Trp53*$^{Y217C/Y217C}$ MEFs and a moderate increase in untreated and Nutlin-treated *Trp53*$^{+/Y217C}$ MEFs, compared to WT cells (Figures 2A and S2). Protein levels for p21 and Mdm2, the products of two classical p53 target genes, appeared similar in *Trp53*$^{+/+}$ and *Trp53*$^{+/Y217C}$ MEFs, and were undetectable or markedly decreased in *Trp53*$^{Y217C/Y217C}$ and *Trp53*$^{-/-}$ MEFs (Figures 2A and S2). Accordingly, p53^{Y217C} appeared unable to transactivate the *Cdkn1a/p21* and *Mdm2* genes or to bind their promoters (Figure 2B). The fractionation of cells before or after treatment with doxorubicin, a clastogenic drug, indicated that p53^{WT} accumulated in the nucleoplasm and chromatin fractions in response to DNA damage, whereas p53^{Y217C} appeared mostly cytoplasmic in both untreated and doxorubicin-treated cells, and undetectable or barely detectable in chromatin fractions (Figures 2C and S3). Furthermore,

when Nutlin-treated MEFs were analyzed by immunofluorescence, $p53^{WT}$ was only detected in nuclei, whereas $p53^{Y217C}$ could be observed in nuclear and cytoplasmic compartments (Figure 2D). We next analyzed two well-known p53-mediated responses to DNA damage, i.e. cell cycle arrest in MEFs and apoptosis in thymocytes (Kastan et al., 1992; Lowe et al., 1993). WT MEFs exposed to increasing doses of ɣ-irradiation (3 Gy or 12 Gy) exhibited significant increases in G1/S ratios, whereas G1/S ratios were similar before or after irradiation in *Trp53*$^{Y217C/Y217C}$ and *Trp53*$^{-/-}$ MEFs (Figures 2E and S4). Furthermore, thymocytes recovered from irradiated WT mice underwent a massive apoptotic response, with an almost three-fold increase in apoptotic cells after a 10 Gy irradiation. By contrast, no increase in apoptotic cells was observable upon irradiation in the thymi from *Trp53*$^{Y217C/Y217C}$ mice, and apoptotic thymocytes were equally rare in irradiated *Trp53*$^{Y217C/Y217C}$ and *Trp*53$^{-/-}$ mice (Figures 2F and S5). Together, these results indicated that the $p53^{Y217C}$ mutation altered the abundance and intracellular distribution of the p53 protein, associated with a decrease in DNA-bound protein, and that $p53^{Y217C}$ had completely lost the ability to induce cell cycle arrest and apoptosis upon DNA damage.

Increased chromosomal instability in *Trp53*$^{Y217C/Y217C}$ cells

We next searched for evidence, at the cellular level, of potential dominant negative effect (DNE) or gain of function (GOF) for the $p53^{Y217C}$ mutant. Little if any difference in the transactivation of canonical p53 target genes was observed between WT, *Trp53*$^{+/Y217C}$ and *Trp53*$^{+/-}$ cells treated with Nutlin or Doxorubicin (Figure S6A), and *Trp53*$^{+/Y217C}$ and *Trp53*$^{+/-}$ cells exhibited similar cell cycle arrest or apoptotic responses to γ-irradiation (Figure S6B-C), suggesting little or no DNE in response to various stresses.

On the opposite, we obtained clear evidence of a GOF for the $p53^{Y217C}$ mutant. Two p53 mutants ($p53^{G245D}$ and $p53^{R273H}$) were recently proposed to promote tumorigenesis by predisposing cells to chromosomal instability (Zhao et al., 2024), which led us to compare the frequency of chromosome rearrangements in WT, *Trp53*$^{Y217C/Y217C}$ and *Trp*53$^{-/-}$ primary MEFs. We searched for chromosome breaks, radial chromosomes, or double-minute chromosomes (DMs) in preparations of MEFs treated with the anti-mitotic nocodazole for metaphase enrichment. The three categories of chromosome rearrangements were more frequently observed in *Trp53*$^{Y217C/Y217C}$ MEFs than in *Trp*53$^{-/-}$ or WT cells (Figure 2G), indicating a GOF that promotes chromosomal instability.

Impact of p53^{Y217C} on mouse development

We next determined the impact of the p53^{Y217C} mutation *in vivo*, by comparing mouse cohorts generated from intercrosses of heterozygous *Trp53*$^{+/-}$ or *Trp53*$^{+/Y217C}$ mice resulting from ≥ 5 backcrosses to the C57BL6/J background. Intercrosses of *Trp53*$^{+/-}$ mice are known to yield a reduced proportion of *Trp53*$^{-/-}$ mice, that is mainly due to defects in neural tube closure causing exencephaly in a fraction of *Trp53*$^{-/-}$ female embryos (Armstrong et al., 1995; Sah et al., 1995) and, to a lesser extent, to lung dysfunction affecting a fraction of *Trp53*$^{-/-}$ neonates (Tateossian et al., 2015). At weaning (on the 21st day postpartum or P21), we observed one *Trp53*$^{-/-}$ female mouse for 3.5 p53$^{-/-}$ males from *Trp53*$^{+/-}$ intercrosses, an underrepresentation of females consistent with frequencies reported in earlier studies (Armstrong et al., 1995; Sah et al., 1995). Strikingly, the underrepresentation of weaned females was even more acute for *Trp53*$^{Y217C/Y217C}$ mice, with only one *Trp53*$^{Y217C/Y217C}$ female for 19 *Trp53*$^{Y217C/Y217C}$ males from *Trp53*$^{+/Y217C}$ intercrosses (Figure 3A). We next analyzed *Trp53*$^{Y217C/Y217C}$ embryos generated from heterozygous intercrosses or from heterozygous-homozygous (*Trp53*$^{+/Y217C}$ x *Trp53*$^{Y217C/Y217C}$) crosses, at embryonic days E12.5-E16.5. An underrepresentation of *Trp53*$^{Y217C/Y217C}$ female embryos was not observed, but 11/26 (42%) female embryos exhibited developmental abnormalities, including 10 with exencephaly, whereas all the male embryos appeared normal (Figure 3B). Importantly, the frequency of *Trp53*$^{Y217C/Y217C}$ female embryos with exencephaly (38.5%) was much higher than the reported frequency (0-8%) of *Trp53*$^{-/-}$ female embryos with exencephaly of C57BL/6 x 129/Sv genetic background (Donehower et al., 1992; Sah et al., 1995), suggesting a stronger effect of the p53^{Y217C} mutant on female embryonic development.

In *Trp53*$^{-/-}$ female mice, exencephaly was previously correlated with stochastic aberrant X chromosome inactivation, with a decreased expression of *Xist* and an increase in bi-allelic expression of X-linked genes including *Maob*, *Pls3* and *Usp9x* (Delbridge et al., 2019). We prepared neurospheres from *Trp53*$^{+/+}$, *Trp53*$^{-/-}$ and *Trp53*$^{Y217C/Y217C}$ female embryos and quantified mRNAs for these genes in neurospheres. Compared to neurospheres from WT animals, *Trp53*$^{Y217C/Y217C}$ and *Trp53*$^{-/-}$ neurospheres exhibited an apparent decrease in *Xist* expression and significantly higher levels of *Maob*, *Pls3* and *Usp9x* (Figure S7). Thus, as for female *Trp53*$^{-/-}$ mice, aberrant chromosome X inactivation may contribute to the underrepresentation of *Trp53*$^{Y217C/Y217C}$

female mice. Of note however, defects in chromosome X inactivation did not appear more pronounced in *Trp53*$^{Y217C/Y217C}$ neurospheres than in *Trp53*$^{-/-}$ neurospheres.

To further analyze the impact of the p53^{Y217C} mutation during development, we also determined its potential effect in embryos lacking Mdm2 or Mdm4, two major p53 regulators. The embryonic lethality resulting from Mdm2 or Mdm4 loss is rescued by a concomitant p53 deficiency (Bardot et al., 2015; Finch et al., 2002; Jones et al., 1995; Migliorini et al., 2002; Montes de Oca Luna et al., 1995; Parant et al., 2001). This provides a powerful assay for analyzing the functionality of p53 mutant alleles (Bardot et al., 2015; Iwakuma et al., 2004; Marine et al., 2006; Toledo et al., 2006). We identified *Mdm2*$^{-/-}$ *Trp53*$^{Y217C/Y217C}$ and *Mdm4*$^{-/-}$ *Trp53*$^{Y217C/Y217C}$ viable mice of both sexes, consistent with a major loss of canonical WT p53 activities in the p53^{Y217C} mutant (Table S1). Of note, in these experiments we mated *Mdm4*$^{+/-}$ *Trp53*$^{+/Y217C}$ mice with *Mdm4*$^{+/-}$ *Trp53*$^{Y217C/Y217C}$ mice, or *Mdm2*$^{+/-}$ *Trp53*$^{+/Y217C}$ mice with either *Mdm2*$^{-/-}$ *Trp53*$^{Y217C/Y217C}$ or *Mdm2*$^{+/-}$ *Trp53*$^{Y217C/Y217C}$ animals, to analyze the progeny at weaning. No *Trp53*$^{Y217C/Y217C}$ female mouse was recovered from these crosses, whereas 14 *Trp53*$^{Y217C/Y217C}$ males were obtained, again demonstrating a striking deficit in *Trp53*$^{Y217C/Y217C}$ females at weaning. Among animals lacking one or two copies of either *Mdm2* or *Mdm4*, we also observed a deficit in *Trp53*$^{Y217C/Y217C}$ weaned females. However, the female to male ratio for *Trp53*$^{Y217C/Y217C}$ animals appeared markedly increased in genetic backgrounds with *Mdm4* haploinsufficiency (4/15) or loss (1/6), but only marginally increased (if at all) in genetic backgrounds with *Mdm2* haploinsufficiency (1/11) or loss (1/11). This suggested that altering the levels of p53 inhibitors, particularly Mdm4, might improve the survival of *Trp53*$^{Y217C/Y217C}$ females (Table S1).

The high frequency (42%) of abnormal *Trp53*$^{Y217C/Y217C}$ female embryos at E12.5-E16.5 could only partially account for the acute deficit in *Trp53*$^{Y217C/Y217C}$ females observed at weaning, suggesting either embryonic abnormalities undetectable macroscopically, or that a fraction of *Trp53*$^{Y217C/Y217C}$ females died later in development or postpartum. We performed additional crosses to analyze female to male ratios at postpartum day 0 or 1 (P0-P1) and observed 20 females for 18 males for *Trp53*$^{+/+}$ animals, but only five females for 22 males for *Trp53*$^{Y217C/Y217C}$ animals (Figure 3C). Furthermore, only one of these *Trp53*$^{Y217C/Y217C}$ females reached weaning age, and the four other neonates died before P2. Altogether, these data led to conclude that the p53^{Y217C} mutation caused female-specific developmental abnormalities at a higher penetrance than a null

allele, leading to a perinatal (late embryonic or early postpartum) lethality for most homozygous mutant females.

Interestingly, we observed that *Trp*53$^{Y217C/Y217C}$ males were fertile and included them in some of our crosses to generate homozygous mutants at higher frequencies (Figure 3B-C). By contrast, we were able to mate two *Trp53*$^{Y217C/Y217C}$ adult females with a *Trp53*$^{+/Y217C}$ male, and both got pregnant but had to be euthanized due to complications while giving birth. In both cases, extended labor (> 24 hr) was the main sign of dystocia (Table S2). These observations suggest that, even for the rare *Trp53*$^{Y217C/Y217C}$ females able to reach adulthood, the p53^{Y217C} mutation caused pathological traits not observed in *Trp53*$^{-/-}$ females, because the loss of p53 was not previously reported to cause dystocia (Embree-Ku and Boekelheide, 2002; Guimond et al., 1996; Hu et al., 2007). Together, our data indicated that the p53^{Y217C} mutation not only abolished canonical p53 activities, but also conferred additional effects compromising female perinatal viability or parturition.

Impact of p53^{Y217C} on tumorigenesis

We next analyzed the impact of the p53^{Y217C} mutation on the onset and spectrum of spontaneous tumors in mice. We first compared *Trp53*$^{+/Y217C}$, *Trp53*$^{+/-}$ and *Trp53*$^{+/+}$ mouse cohorts for 2 years. *Trp53*$^{+/Y217C}$ and *Trp53*$^{+/-}$ cohorts exhibited similar spontaneous tumor onset and spectrum, with most mice developing sarcomas during their second year of life (Figure S8). Thus, at least for tumors arising spontaneously, the p53^{Y217C} mutant protein did not appear to exert a DNE over the wildtype p53 protein.

We next compared *Trp53*$^{Y217C/Y217C}$ and *Trp53*$^{-/-}$ mouse cohorts. Because of the difficulty to generate *Trp53*$^{Y217C/Y217C}$ females, we restricted our comparison to males, to avoid potential biases that might result from different sex ratios. All *Trp53*$^{-/-}$ mice are known to die in less than 1 year, from thymic lymphomas in most cases, or more rarely from sarcomas (Donehower et al., 1992; Jacks et al., 1994). *Trp53*$^{Y217C/Y217C}$ males died faster than their *Trp53*$^{-/-}$ counterparts: all the *Trp53*$^{Y217C/Y217C}$ males were dead by the age of 7 months, whereas more than 20% of the *Trp53*$^{-/-}$ males were still alive at that age (Figure 4A). Furthermore, most *Trp53*$^{-/-}$ and *Trp53*$^{Y217C/Y217C}$ mice died from thymic lymphomas, but histological analysis of tumor organs revealed that the lymphomas in *Trp53*$^{Y217C/Y217C}$ males were more aggressive and invasive, with sites of metastases notably including the lungs, spleen, liver or kidneys (Figures 4B-C and S9). Thus, the p53^{Y217C}

mutation not only abolished canonical tumor suppressive activities but also apparently conferred oncogenic properties to the encoded protein. Consistent with this, when we performed an RNA-seq analysis of thymi from 8 weeks-old *Trp53*$^{+/+}$, *Trp53*$^{-/-}$ and *Trp53*$^{Y217C/Y217C}$ males, 81.5 % of the 717 differentially expressed genes indicated a loss of function (LOF) in the p53^{Y217C} mutant, but genes suggesting a GOF or a separation of function (SOF) were also observed (Figure S10A and Table S3). Of note, among the differentially expressed genes corresponding to a LOF in the p53^{Y217C} mutant were *Bbc3/Puma*, *Cdkn1a/p21* and *Zmat3* (Figure S10B), three p53-target genes known to play major roles in p53-mediated tumor suppression (Brennan et al., 2023).

We next performed a comparative analysis focusing on *Trp53*$^{Y217C/Y217C}$ and *Trp53*$^{-/-}$ thymi, which revealed 192 differentially expressed genes (Figure 5A-B and Table S4). An analysis of these data with GOrilla, the Gene Ontology enRIchment anaLysis and visuaLizAtion tool (Eden et al., 2009), indicated that 141 of these genes were associated with at least one gene ontology (GO) term, and revealed a significant enrichment for genes associated with white blood cell chemotaxis/migration and inflammation (Figures 5C and S11). Among these genes were notably *Ccl17*, *Ccl9*, *Ccr3*, *Cxcl10*, *S100a8* and *S100a9*, six genes associated each with 10-15 GO terms related to white blood cell behavior and inflammation (Table S5). We next used RT-qPCR to quantify the expression of these genes in thymi from 8 weeks-old *Trp53*$^{+/+}$, *Trp53*$^{Y217C/Y217C}$ and *Trp53*$^{-/-}$ male mice. Their expression was significantly increased in *Trp53*$^{Y217C/Y217C}$ thymic cells compared to *Trp53*$^{-/-}$, or to both *Trp53*$^{+/+}$ and *Trp53*$^{-/-}$ cells, consistent with gain or separation of function (GOF/SOF) effects in the *Trp53*^{Y217C} mutant (Figure 5D). We also compared the transcriptomes of *Trp53*$^{Y217C/Y217C}$ and *Trp53*$^{-/-}$ thymocytes by gene set enrichment analysis (Subramanian et al., 2005). We found 13 gene sets significantly enriched in *Trp53*$^{Y217C/Y217C}$ cells with normalized enrichment scores (NES) > 2, among which three ("antimicrobial peptides", "chemokine receptors bind chemokines" and "defensins") were related to immunity (Figures 5E and S12A), consistent with an inflammatory response associated with the p53^{Y217C} mutant. Other enriched gene sets notably included five sets ("electron transport chain", "respiratory electron transport ATP synthesis by chemiosmotic coupling and heat production by uncoupling proteins", "mitochondrial translation", "respiratory electron transport" and "oxidative phosphorylation") related to mitochondria function, and three sets ("deposition of new CENPA-containing nucleosomes at the centromere", "arginine methyltransferases methylate histone arginines" and "PRC2 methylates histones and DNA") related to chromatin plasticity (Figures 5E and S12B-C).

These gene sets, differentially expressed between *Trp53*$^{Y217C/Y217C}$ and *Trp53*$^{-/-}$ cells, might contribute to accelerated tumorigenesis in *Trp53*$^{Y217C/Y217C}$ mice, given the reported impact of inflammation, metabolism changes and epigenetic plasticity on cancer evolution (Feinberg et al., 2006; Greten and Grivennikov, 2019; Kroemer and Pouyssegur, 2008). Furthermore, the hotspot mutants p53^{G245D} or p53^{R273H} were recently proposed to promote tumor progression by inducing non-canonical nuclear factor kappa light chain enhancer of activated B cell (NC-NF-κB) signaling (Zhao et al., 2024). In *Trp53*$^{Y217C/Y217C}$ cells, one gene set related to NC-NF-κB ("Dectin 1-mediated non-canonical NF-κB signaling") was significantly enriched and two other NF-κB-related gene sets were also potentially enriched (Figure 5F and S13).

Reducing inflammation may rescue a fraction of female *Trp53*$^{Y217C/Y217C}$ embryos

Our data indicated that inflammation correlated with accelerated tumorigenesis in *Trp53*$^{Y217C/Y217C}$ male mice. Interestingly, inflammation was previously proposed to promote neural tube defects or embryonic death in a few mouse models (Lian et al., 2004; McNairn et al., 2019; Zhao et al., 2013). Furthermore *CD44*, encoding a cell-surface glycoprotein that drives inflammation and cancer progression (Solier et al., 2023), was recently identified as a key gene for the diagnosis and early detection of open neural tube defects (Karthik et al., 2022). Together, these data led us to hypothesize that, at least in a fraction of *Trp53*$^{Y217C/Y217C}$ females, neural tube defects might result from inflammation. To test this hypothesis, we mated *Trp53*$^{+/Y217C}$ female mice with *Trp53*$^{Y217C/Y217C}$ males, then administered supformin to pregnant females by oral gavage. Supformin (LCC-12), a potent inhibitor of the CD44-copper signaling pathway, was shown to reduce inflammation *in vivo* (Solier et al., 2023). Without any treatment, our previous crosses (Figure 3 and Table S1) collectively yielded a female to male ratio of 0.045 for *Trp53*$^{Y217C/Y217C}$ weaned mice (f/m=5/111 [4+1+0+0]/[75+22+9+5]), significantly different from the ratio of 0.29 (f/m=8/28) for *Trp53*$^{-/-}$ weaned animals. By contrast, in the progeny of supformin-treated pregnant mice we observed a five-fold increase in the female to male ratio for *Trp53*$^{Y217C/Y217C}$ weaned animals, to reach a value of 0.23 (f/m=3/13) indistinguishable from the ratio in *Trp53*$^{-/-}$ weaned animals from untreated mice (Figure 5G and Table S6). This result suggests that reducing inflammation in developing *Trp53*$^{Y217C/Y217C}$ female embryos may increase their viability.

Discussion

In this report, we generated a mouse model with a *Trp53*^{Y217C} allele, the murine equivalent of the human hotspot mutant *TP53*^{Y220C}. The analysis of this mouse model indicated that the p53^{Y217C} mutation leads to the loss of many canonical wildtype p53 activities, notably the capacity to transactivate target genes important for tumor suppression (e.g. *Bbc3*, *Cdkn1a* and *Zmat3*). The fact that p53^{Y217C} can rescue the embryonic lethality caused by a deficiency in Mdm2 or Mdm4 is also consistent with a major loss of canonical wildtype p53 functions (LOF) in this mutant. These findings are consistent with the notion that hotspot p53 mutants cause a complete or near complete LOF (Funk et al., 2025).

In addition, our analyses provide evidence that the p53^{Y217C} mutation exhibits oncogenic effects. The possibility that a mutant p53 might acquire oncogenic functions was first suggested over 30 years ago (Dittmer et al., 1993), but this notion became controversial in recent years. Indeed, studies of a few p53 mutants in human acute myeloid leukemia and a mouse model of B cell lymphoma indicated that their increased tumorigenicity might result from dominant-negative effects (DNE) rather than gain of function (GOF), and a recent study further suggested that the putative GOF of many p53 mutants would not be required to sustain the expansion of tumors (Aubrey et al., 2018; Boettcher et al., 2019; Wang et al., 2023). Here, however, we observed accelerated tumorigenesis in *Trp53*$^{Y217C/Y217C}$ mice, but did not observe any evidence of DNE for spontaneous tumorigenesis in *Trp53*$^{+/Y217C}$ animals. Importantly, the fact that p53^{Y217C} did not exhibit a DNE over the WT protein is consistent with the report that Li-Fraumeni patients carrying an heterozygous *TP53*^{Y220C} mutation display a similar age of cancer onset than Li-Fraumeni patients with an heterozygous non-sense *TP53* mutation (Xu et al., 2014). Furthermore, our evidence of an oncogenic GOF leading to aggressive metastatic tumors in *Trp53*$^{Y217C/Y217C}$ male mice is consistent with the oncogenic GOF attributed to p53^{Y220C} in male patients with glioblastoma (Rockwell et al., 2021) or with experiments suggesting that p53^{Y220C} expression in p53-null cells, or its overexpression in MCF-10A cells, may increase their migratory or invasive capacities (Pal et al., 2023; Zhou et al., 2022).

Our transcriptomic analyses suggested that the p53^{Y217C} mutant might accelerate tumorigenesis by promoting inflammation, a hallmark of cancer (Hanahan, 2022) previously associated with a few other hotspot p53 mutants with oncogenic GOF (Agupitan et al., 2020;

Behring et al., 2019; Ham et al., 2019; Zhao et al., 2024). Interestingly, the GSEA comparison of transcriptomes from *Trp53*$^{Y217C/Y217C}$ and *Trp*53$^{-/-}$ male thymic cells indicated differences related to inflammation and chemokine signaling, but also to mitochondria function and chromatin plasticity, and a link between inflammation, mitochondrial copper and epigenetic plasticity was recently demonstrated (Solier et al., 2023). Furthermore, the p53^{G245D} or p53^{R273H} mutants were proposed to accelerate tumorigenesis by promoting a chromosomal instability that would activate NC-NF-kB signaling and promote tumor cell metastasis (Zhao et al., 2024). Here we observed increased chromosomal instability in *Trp53*$^{Y217C/Y217C}$ fibroblasts, increased NC-NF-kB and inflammation-related signaling in *Trp53*$^{Y217C/Y217C}$ thymocytes, and increased tumor metastasis in *Trp53*$^{Y217C/Y217C}$ mice compared to their *Trp53*$^{-/-}$ counterparts. These data suggest that similar mechanisms might underlie the oncogenic properties of the p53^{Y217C}, p53^{G245D} and p53^{R273H} mutants.

A striking and unexpected effect of the p53^{Y217C} mutation was its severe impact on the perinatal viability of female mice, which led to observe only four *Trp53*$^{Y217C/Y217C}$ females for 75 *Trp53*$^{Y217C/Y217C}$ males at weaning from heterozygous intercrosses, or five *Trp53*$^{Y217C/Y217C}$ females for 111 *Trp53*$^{Y217C/Y217C}$ males when all weaned animals from relevant crosses were considered. The perinatal lethality of *Trp53*$^{Y217C/Y217C}$ females correlated with a high frequency (38.5%) of exencephalic females at E12.5-E16.5 embryonic ages. By comparison, the female to male ratio at weaning was 8/28 for *Trp53*$^{-/-}$ mice, and only 0-8% of exencephalic female *Trp53*$^{-/-}$ embryos were reported in similar genetic backgrounds (Armstrong et al., 1995; Donehower et al., 1992; Sah et al., 1995). These observations provide evidence of teratogenic effects for the p53^{Y217C} mutant protein. Three other mouse p53 models were previously found to cause exencephaly at a higher frequency than a p53 null allele : *Trp53*^{NLS1}, with 3 mutations at residues 316-318 affecting a nuclear localization signal and leading to a predominantly cytoplasmic localization of p53^{NLS1} in most cells (Regeling et al., 2011); *Trp53*^{N236S}, a mouse model of *TP53*^{N239S}, a recurrent but uncommon mutant in human cancers (Zhao et al., 2019); and *Bim*$^{+/-}$ *Trp53*$^{-/-}$ mice, combining p53 loss with an haploinsufficiency in the cytoplasmic proapoptotic regulator Bim/Bcl2l11 (Delbridge et al., 2019). The female-specific lethality of *Trp53*^{N236S} mice was proposed to result from increased *Xist* expression, whereas a decrease in *Xist* expression was observed in *Bim*$^{+/-}$ *Trp53*$^{-/-}$ mice, suggesting distinct causes for neural tube defects (Delbridge et al., 2019; Zhao et al., 2019). We observed decreased *Xist* expression and an increased expression of X-linked genes in

neurospheres from *Trp53*$^{Y217C/Y217C}$ females compared to WT females, whereas these genes were expressed at similar levels in neurospheres from *Trp53*$^{Y217C/Y217C}$ and *Trp53*$^{-/-}$ females. These results are not consistent with the mechanism proposed for exencephaly in the *Trp53*^{N236S} mouse model, but might rather reflect a p53 LOF in *Trp53*$^{Y217C/Y217C}$ embryos. In addition, the analyses of the *Trp53*^{NLS1} and *Bim*$^{+/-}$ *Trp53*$^{-/-}$ mouse models make it tempting to speculate that, in female *Trp53*$^{Y217C/Y217C}$ embryos, the abundance of p53^{Y217C} in the cytoplasm might perturb mitochondria function (Blandino et al., 2020) to further promote neural tube closure defects. Consistent with this possibility, p53 mutant proteins accumulating in the cytoplasm were reported to inhibit autophagy (Morselli et al., 2008), a key determinant for mitochondrial integrity (Rambold and Lippincott-Schwartz, 2011), and autophagy impairment may promote neural tube defects (Fimia et al., 2007; Ye et al., 2020).

Importantly, our data suggest that common mechanisms might contribute to the oncogenic effects accelerating tumorigenesis in *Trp53*$^{Y217C/Y217C}$ males and the teratogenic effects causing the perinatal lethality of many *Trp53*$^{Y217C/Y217C}$ females. Indeed, the RNAseq analysis of male thymocytes indicated that inflammation likely promotes oncogenesis in *Trp53*$^{Y217C/Y217C}$ males, and the administration of the anti-inflammatory drug supformin to pregnant mice increased the ratio of *Trp53*$^{Y217C/Y217C}$ weaned females in their progeny. Thus, the low female/male ratio observed for *Trp53*$^{Y217C/Y217C}$ weaned animals would likely result not only from aberrant X-chromosome inactivation in female embryos as in *Trp53*$^{-/-}$ animals (Delbridge et al., 2019), but also from inflammation. Presumably, a higher level of chromosomal instability in *Trp53*$^{Y217C/Y217C}$ cells might promote inflammation in *Trp53*$^{Y217C/Y217C}$ embryos (Rodier et al., 2009), and this might be more detrimental to females because *Trp53*$^{Y217C/Y217C}$ males would be protected by the anti-inflammatory effects of androgens (Ainslie et al., 2024; Bianchi, 2019; McNairn et al., 2019). Of note, we also observed that decreased Mdm4 levels increased the female/male ratio in *Trp53*$^{Y217C/Y217C}$ weaned mice. Because MDM4 overexpression was shown to promote genome instability and inflammation in cells independently of p53 (Carrillo et al., 2015; Liu et al., 2024), it is tempting to speculate that, as for supformin-treated mice, the improved survival of *Trp53*$^{Y217C/Y217C}$ female embryos in an Mdm4$^{+/-}$ background might result from decreased inflammation. Interestingly, in the offspring of human pregnancies at risk of early preterm delivery, an Interleukin-6 polymorphism was associated with a female-specific susceptibility to adverse neurodevelopmental outcome (Varner et al., 2020), suggesting that inflammation may also

impact the development of human female embryos. Finally, our mating attempts with *Trp53*$^{Y217C/Y217C}$ mice indicated that *Trp53*$^{Y217C/Y217C}$ pregnant females exhibited dystocia, and parturition is considered to be a finely regulated inflammatory process (Zhang and Wei, 2021). Of note, dystocia was not observed in *Trp53*$^{-/-}$ mice, but was previously reported in pregnant females with a combined deficiency of p53 and FasL (Embree-Ku and Boekelheide, 2002). The fact that *Trp53*$^{Y217C/Y217C}$ females shared phenotypic traits with both *Bim*$^{+/-}$ *Trp53*$^{-/-}$ mice (neural tube defects) and *FasL*$^{-/-}$ *Trp53*$^{-/-}$ mice (dystocia) may seem relevant, because Bim and FasL are both regulators of apoptosis and autophagy that also regulate immune responses (Sionov et al., 2015; Taylor and Ng, 2018). Altogether, these data suggest that inflammation may cause accelerated tumorigenesis in *Trp53*$^{Y217C/Y217C}$ male mice and contribute to promote neural tube defects in *Trp53*$^{Y217C/Y217C}$ female embryos or dystocia in *Trp53*$^{Y217C/Y217C}$ pregnant females (Table S7).

In conclusion, we generated a mouse model expressing p53^{Y217C}, the murine equivalent of human p53^{Y220C}, and its analysis revealed that the gain-of-function of a hotspot mutant p53 may not be limited to oncogenic effects. This is an important notion to consider given the ever-expanding functions ascribed to p53 (Hu, 2009; Rakotopare and Toledo, 2023; Voskarides and Giannopoulou, 2023; Vousden and Lane, 2007). In addition, our results unveiled the potential relevance of supformin in obstetrics, which deserves further investigation.

Materials and Methods

LSL-Y217C construct

We used mouse genomic *Trp53* DNA from previous constructs, containing a portion of intron 1 with a LoxP-Stop-LoxP (LSL) cassette (Ventura et al., 2007) in which the puromycin-resistance gene was replaced by a neomycin-resistance gene (Simeonova et al., 2013). The point mutation (A to G) encoding a Tyr to Cys substitution (TAT to TGT) at codon 217, together with a silent mutation nearby creating a Ban II restriction site, were introduced by PCR directed mutagenesis by using primers Y217C-F and Y217C-R (See Table S8 for primer sequences). The resulting *Trp53*$^{\text{LSL-Y217C}}$ targeting vector was fully sequenced before use.

Targeting in ES Cells and Genotyping

129/SvJ embryonic stem (ES) cells were electroporated with the targeting construct linearized with Not I. Two recombinant clones, identified by long-range PCR and confirmed by internal PCR and Southern Blot, were injected into C57BL/6J blastocysts to generate chimeras, and germline transmission was verified by genotyping their offspring. *In vivo* excision of the LSL cassette was performed by breeding *Trp53*$^{+/\text{LSL-Y217C}}$ male mice with females carrying the PGK-*Cre* transgene (Lallemand et al., 1998) and genotyping their offspring. The *Trp53*$^{\text{Y217C}}$ (p53^{YC}) mutation was routinely genotyped by PCR using primers c and d (Figure 1, Table S8) followed by BanII digestion. Tumorigenesis studies were performed on mouse cohorts resulting from ≥ 5 generations of backcrosses with C57BL6/J mice. For all experiments, mice housing and treatment were conducted according to the Institutional Animal Care and Use Committee of the Institut Curie (approved project #03769.02).

Cells and Cell Culture Reagents

Mouse embryonic fibroblasts (MEFs) isolated from 13.5-day embryos were cultured in a 5% CO2 and 3% O2 incubator, in DMEM GlutaMAX (Gibco), with 15% FBS (Biowest), 100 μM 2-mercaptoethanol (Millipore), 0.01 mM Non-Essential Amino-Acids, and penicillin/streptomycin (Gibco) for ≤ 6 passages. Cells were irradiated with a Cs γ-irradiator or treated for 24 hr with 10 μM Nutlin 3a (Sigma-Aldrich) or 1 μM Doxorubicin (Sigma-Aldrich). Neurospheres were prepared by isolating neural stem/progenitor cells (NPCs) from the lateral and median ganglionic

eminences of E14.5 embryos. NPCs were cultured in a 5% CO_2 incubator, in DMEM/F12 medium (with L-Glutamine, Invitrogen) supplemented with 1% B-27 (Invitrogen), 1% N2 (Invitrogen), 0.3% glucose (Invitrogen), 25 μg/ml insulin (Sigma-Aldrich), 20 ng/ml EGF (PeproTech), 10 ng/ml bFGF (PeproTech) and penicillin/streptomycin (Gibco). Neurospheres were dissociated once a week by Accutase treatment and mechanically, then seeded at 10^6 cells per 6 cm diameter dish.

Quantitative RT-PCR

Total RNA, extracted using NucleoSpin RNA II (Macherey-Nagel), was reverse transcribed using SuperScript IV (Invitrogen). Real-time quantitative PCRs were performed as previously described (Simeonova et al., 2012), on an ABI PRISM 7500 using Power SYBR Green (Applied Biosystems). Primer sequences are reported in Table S8.

Western Blots

Cells were lysed in RIPA buffer (50 mM Tris-HCl pH 8, 150 mM NaCl, 5 mM EDTA, 0.5% deoxycholic acid, 0.1% SDS, 1% NP-40) supplemented with Protease inhibitors cocktail (Roche) and 1 mM PMSF (Sigma). Whole-cell extracts were sonicated three times for 10 s and centrifuged at 13 000 rpm for 30 min to remove cell debris. Protein lysate concentration was determined by BCA assay (Thermo Scientific) and 30 μg of each lysate was fractionated by SDS–PAGE on a 4-12% polyacrylamide gel and transferred onto polyvynilidene difluoride (PVDF) membranes (Amersham). Membranes were incubated with antibodies raised against Mdm2 (MDM2-4B2, Abcam, 1/500), p53 (CM-5, Novocastra, 1/2000), p21 (F5, Santa Cruz Biotechnology, 1/200) and actin (actin-HRP sc47778, Santa Cruz Biotechnology, 1/5000). Chemiluminescence revelation of western blots was achieved with the SuperSignal West Dura (Perbio).

ChIP Assay

ChIP analysis was performed as previously described (Simeonova et al., 2013). p53-DNA complexes were immunoprecipitated from total extracts by using 50 μg of a polyclonal antibody against p53 (FL-393, Santa Cruz Biotechnology) and 300 μg of sonicated chromatin. Rabbit IgG (Abcam) was used for control precipitation. Quantitative PCR was performed on ABI PRISM 7500. Primer sequences are reported in Table S8.

Cell Fractionation Assay

Cells were lysed in hypotonic lysis buffer (10 mM Tris pH 7.5, 10 mM NaCl, 3 mM Mgcl2, 0.3% NP-40, 10% glycerol) on ice for 10 min, then centrifuged at 4°C for 3 min at 1000g. The supernatant was recovered as the cytoplasmic fraction, and the pellet was incubated in a modified Wuarin-Schibler buffer (10 mM Tris-HCl pH 7.0, 4 mM EDTA, 0.3 M NaCl, 1 M urea, 1% NP-40) on ice for 5 min, vortexed, incubated on ice for 10 min, then centrifuged at 4°C for 3 min at 1000g. The supernatant was recovered as the nucleoplasmic fraction, and the pellet was washed, then incubated in a nuclear lysis buffer (20 mM Tris pH 7.5, 150 mM KCl, 3 mM MgCl2, 0.3% NP-40, 10% glycerol) on ice for 5 min, sonicated, then centrifuged at 13000 rpm at 4°C and the supernatant was recovered as the chromatin fraction. All buffers were supplemented with Protease inhibitors cocktail (Roche). Cellular fractions were analyzed by western blots with antibodies against p53 (AF-1355, R&D systems, 1/600), Tubulin (ab15568, Abcam, 1/1000), Nup98 (ab50610, Abcam, 1/1000) and histone H3 (ab1791, Abcam, 1/1000). Chemiluminescence revelation was achieved with SuperSignal West Pico or Femto (Thermoscientific) and analyzed with a ChemiDoc imaging system (Bio-Rad).

Immunofluorescence

MEFs were cultured on collagen-coated coverslips, treated with 10 μM Nutlin 3a (Sigma-Aldrich) for 24 hr and analyzed. Coverslips were stained with rabbit anti-p53 FL-393 (Santa Cruz Biotechnology, 1/50), mouse anti-actin primary antibody and with Alexa Fluor 647 anti-Rabbit and Alexa Fluor 488 anti-Mouse secondary antibodies (Molecular Probes). DNA was counterstained with DAPI. Images were captured on an epifluorescence microscope using equal exposure times for all images for each fluor.

Cell-Cycle Assay

Log phase cells were irradiated at room temperature (RT) with a Cs γ-irradiator at doses of 3 or 12 Gy, incubated for 24 hr, then pulse labeled for 1 hr with BrdU (10 μM), fixed in 70% ethanol, double stained with FITC anti-BrdU and propidium iodide, and analyzed by flow cytometry with a BD Biosciences FACSort and the FlowJo software.

Apoptosis Assay

Six to eight weeks-old mice were left untreated or submitted to 10 Gy whole-body ɣ-irradiation. Mice were sacrificed 4 hr later and thymi were extracted. Thymocytes were recovered by filtration through a 70 µm smash, stained with Annexin V-FITC Apoptosis detection kit (Abcam) and propidium iodide, then analyzed with a LSRII FACS machine. Data were analyzed using Flowjo software.

Metaphase spread preparation and analysis

Primary MEFs (at passage 4 for all genotypes) were treated with 0.1 mM nocodazole for 3 h to arrest cells in metaphase, then submitted to hypotonic shock (75 mM KCl), fixed in a (3:1) ethanol/acetic acid solution, dropped onto glass slides, then air-dried slides were stained with Giemsa to score for chromosome aberrations. Images were acquired using a Zeiss Axiophot (X63) microscope.

Histology

Organs were fixed in formol 4% for 24 hr, then ethanol 70%, and embedded in paraffin wax. Serial sections of 3 µm were stained as described (Simeonova et al., 2013), with hematoxylin and eosin using standard procedures.

RNA-Seq analysis

Total RNA was extracted from the thymi of 8 weeks-old asymptomatic male mice using nucleospin RNA II (Macherey-Nagel). The quality of RNA was checked with Bioanalyzer Agilent 2100 and RNAs with a RIN (RNA integrity number) $\geq$ 7 were retained for further analysis. RNA was depleted from ribosomal RNA, then converted into cDNA libraries using a TruSeq Stranded Total Library preparation kit (Illumina). Paired-end sequencing was performed on an Illumina MiSeq platform. Reads were mapped to the mouse genome version GRCm38 and counted on gene annotation gencode.vM18 with featureCounts (Liao et al., 2014). Differentially expressed genes with an adjusted p-value < 0.05 were identified using the DESeq2 R package (Love et al., 2014).

Gene Ontology analysis

Gene ontology analysis of differentially expressed genes was performed by using the GOrilla (Technion) software as previously described (Rakotopare et al., 2023). Enrichment analyses were carried out by comparing the list of 192 differentially expressed genes between *Trp53*$^{Y217C/Y217C}$ and *Trp53*$^{-/-}$ thymi to the full list of genes (background), with ontology searches for biological processes and default *P*-value settings (10^{-3}).

Gene set enrichment analysis

Gene set enrichment analysis was performed by using the GSEA software with canonical pathway gene sets from the Mouse Molecular Signature Database (MSigDB) (Subramanian et al., 2005). Gene sets with a false discovery rate (FDR) q-value < 0.25 were regarded as potentially relevant. The best candidates, with an FDR q-value < 0.01, exhibited normalized enrichment scores (NES) > 1.91 and nominal (NOM) P-values <0.003.

Oral gavage of pregnant females

Trp53$^{+/Y217C}$ female mice were mated with *Trp53*$^{Y217C/Y217C}$ males, then mice with a vaginal plug on the next day were separated from males and weighted every other day to confirm pregnancy. On the 10th and 11th days post-coitum, pregnant mice received 5 mg/kg of supformin (in a PBS solution) by oral gavage with flexible gauge feeding tubes, then their pups were genotyped at weaning.

Statistical analyses

Unless noted otherwise, we used a Student's *t* test to analyze differences between two groups of values. For the proportions of mice at weaning, the observed mouse count was compared to the expected count according to Mendel's distribution and a Chi-square (χ^2) test, and a Fischer's test was applied to compare frequencies of mutant females or female to male ratios. Fischer's tests were also used to analyze frequencies of chromosome rearrangements in fibroblasts. Survival curves were analyzed with log-rank Mantel-Cox tests. Analyses were performed by using GraphPad Prism, and values of $P \leq 0.05$ were considered significant.

Data availability

RNA sequencing data have been deposited in the Gene Expression Omnibus (GEO) under the accession code GSE248936. All other data are available within the article and its supplementary information.

Acknowledgments

This project was supported by grants attributed to F.T., from the Ligue Nationale Contre le Cancer, the Fondation ARC pour la recherche sur le Cancer and the Gefluc. S.J., E.E. and J.R. were PhD fellows of the Ministère de la Recherche, supervised by F.T. (S.J., J.R.) or B.B. (E.E.). S.J. and E.E. received additional support from the Fondation ARC. M.G. was paid by European Research Council 875532-Prostator-ERC-2019-PoC attributed to A.M. For some experiments, S.J. and V.V. received technical assistance from C. Bouyer and R. Bourimi. We thank the following members of the Institut Curie platforms: I. Grandjean, H. Gautier, C. Daviaud, M. Garcia, D. Andreau, M. Verlhac and A. Fosse (animal facility); S. Baulande and S. Lameiras (NGS); M. Huerre, A. Nicolas and R. Leclere (histopathology); Z. Maciorowski, A. Viguier and S. Grondin (flow cytometry).

Author Contributions

Conceptualization: F.T.; investigation: S.J., E.E., J.R., I.S, V.L., V.V., M.L., A.F., B.B., F.T.; formal analysis: M.G., B.B., F.T.; resources: T.C., R.R., A.M.; supervision, writing and visualization: F.T., B.B; project administration and funding acquisition: F.T.

Declaration of interests

The authors declare no competing financial interests.

References

Agupitan AD, Neeson P, Williams S, Howitt J, Haupt S, Haupt Y. 2020. P53: A Guardian of Immunity Becomes Its Saboteur through Mutation. *Int J Mol Sci* **21**:3452. doi:10.3390/ijms21103452

Ainslie RJ, Simitsidellis I, Kirkwood PM, Gibson DA. 2024. RISING STARS: Androgens and immune cell function. *J Endocrinol* **261**:e230398. doi:10.1530/JOE-23-0398

Amelio I, Melino G. 2020. Context is everything: extrinsic signalling and gain-of-function p53 mutants. *Cell Death Discov* **6**:16. doi:10.1038/s41420-020-0251-x

Armstrong JF, Kaufman MH, Harrison DJ, Clarke AR. 1995. High-frequency developmental abnormalities in p53-deficient mice. *Curr Biol* **5**:931–936. doi:10.1016/s0960-9822(95)00183-7

Aubrey BJ, Janic A, Chen Y, Chang C, Lieschke EC, Diepstraten ST, Kueh AJ, Bernardini JP, Dewson G, O'Reilly LA, Whitehead L, Voss AK, Smyth GK, Strasser A, Kelly GL. 2018. Mutant TRP53 exerts a target gene-selective dominant-negative effect to drive tumor development. *Genes Dev* **32**:1420–1429. doi:10.1101/gad.314286.118

Bardot B, Bouarich-Bourimi R, Leemput J, Lejour V, Hamon A, Plancke L, Jochemsen AG, Simeonova I, Fang M, Toledo F. 2015. Mice engineered for an obligatory Mdm4 exon skipping express higher levels of the Mdm4-S isoform but exhibit increased p53 activity. *Oncogene* **34**:2943–2948. doi:10.1038/onc.2014.230

Beckerman R, Prives C. 2010. Transcriptional regulation by p53. *Cold Spring Harb Perspect Biol* **2**:a000935. doi:10.1101/cshperspect.a000935

Behring M, Vazquez AI, Cui X, Irvin MR, Ojesina AI, Agarwal S, Manne U, Shrestha S. 2019. Gain of function in somatic *TP53* mutations is associated with immune-rich breast tumors and changes in tumor-associated macrophages. *Molec Genet Genomic Med* **7**:e1001. doi:10.1002/mgg3.1001

Bianchi VE. 2019. The Anti-Inflammatory Effects of Testosterone. *J Endocr Soc* **3**:91–107. doi:10.1210/js.2018-00186

Blandino G, Valenti F, Sacconi A, Di Agostino S. 2020. Wild type- and mutant p53 proteins in mitochondrial dysfunction: emerging insights in cancer disease. *Semin Cell Dev Biol* **98**:105–117. doi:10.1016/j.semcdb.2019.05.011

Boettcher S, Miller PG, Sharma R, McConkey M, Leventhal M, Krivtsov AV, Giacomelli AO, Wong W, Kim J, Chao S, Kurppa KJ, Yang X, Milenkowic K, Piccioni F, Root DE, Rücker FG, Flamand Y, Neuberg D, Lindsley RC, Jänne PA, Hahn WC, Jacks T, Döhner H, Armstrong SA, Ebert BL. 2019. A dominant-negative effect drives selection of TP53 missense mutations in myeloid malignancies. *Science* **365**:599–604. doi:10.1126/science.aax3649

Bouaoun L, Sonkin D, Ardin M, Hollstein M, Byrnes G, Zavadil J, Olivier M. 2016. TP53 Variations in Human Cancers: New Lessons from the IARC TP53 Database and Genomics Data. *Hum Mutat* **37**:865–876. doi:10.1002/humu.23035

Brennan MS, Brinkmann K, Romero Sola G, Healey G, Gibson L, Gangoda L, Potts MA, Lieschke E, Wilcox S, Strasser A, Herold MJ, Janic A. 2023. Combined absence of TRP53 target genes ZMAT3, PUMA and p21 cause a high incidence of cancer in mice. *Cell Death Differ*. doi:10.1038/s41418-023-01250-w

Carrillo AM, Bouska A, Arrate MP, Eischen CM. 2015. Mdmx promotes genomic instability independent of p53 and Mdm2. *Oncogene* **34**:846–856. doi:10.1038/onc.2014.27

Delbridge ARD, Kueh AJ, Ke F, Zamudio NM, El-Saafin F, Jansz N, Wang G-Y, Iminitoff M, Beck T, Haupt S, Hu Y, May RE, Whitehead L, Tai L, Chiang W, Herold MJ, Haupt Y, Smyth

GK, Thomas T, Blewitt ME, Strasser A, Voss AK. 2019. Loss of p53 Causes Stochastic Aberrant X-Chromosome Inactivation and Female-Specific Neural Tube Defects. *Cell Rep* **27**:442-454.e5. doi:10.1016/j.celrep.2019.03.048

Dibra D, Xiong S, Moyer SM, El-Naggar AK, Qi Y, Su X, Kong EK, Korkut A, Lozano G. 2024. Mutant p53 protects triple-negative breast adenocarcinomas from ferroptosis in vivo. *Sci Adv* **10**:eadk1835. doi:10.1126/sciadv.adk1835

Dittmer D, Pati S, Zambetti G, Chu S, Teresky AK, Moore M, Finlay C, Levine AJ. 1993. Gain of function mutations in p53. *Nat Genet* **4**:42–46. doi:10.1038/ng0593-42

Donehower LA, Harvey M, Slagle BL, McArthur MJ, Montgomery CA, Butel JS, Bradley A. 1992. Mice deficient for p53 are developmentally normal but susceptible to spontaneous tumours. *Nature* **356**:215–221. doi:10.1038/356215a0

Dumbrava E, Johnson M, Tolcher A, Shapiro G, Thompson J, El-Khoueiry A, Vandross A, Kummar S, Parikh A, Munster P, Daly E, De Leon L, Khaddar M, LeDuke K, Robell K, Sheehan L, St. Louis M, Wiebesiek A, Alland L, Schram A. 2022. First-in-human study of PC14586, a small molecule structural corrector of Y220C mutant p53, in patients with advanced solid tumors harboring a TP53 Y220C mutation. *J Clin Oncol* **40**:suppl 3003. doi:10.1200/JCO.2022.40.16_suppl.3003

Eden E, Navon R, Steinfeld I, Lipson D, Yakhini Z. 2009. GOrilla: a tool for discovery and visualization of enriched GO terms in ranked gene lists. *BMC Bioinformatics* **10**:48. doi:10.1186/1471-2105-10-48

Embree-Ku M, Boekelheide K. 2002. Absence of p53 and FasL has sexually dimorphic effects on both development and reproduction. *Exp Biol Med (Maywood)* **227**:545–553. doi:10.1177/153537020222700720

Feinberg AP, Ohlsson R, Henikoff S. 2006. The epigenetic progenitor origin of human cancer. *Nat Rev Genet* **7**:21–33. doi:10.1038/nrg1748

Fimia GM, Stoykova A, Romagnoli A, Giunta L, Di Bartolomeo S, Nardacci R, Corazzari M, Fuoco C, Ucar A, Schwartz P, Gruss P, Piacentini M, Chowdhury K, Cecconi F. 2007. Ambra1 regulates autophagy and development of the nervous system. *Nature* **447**:1121–1125. doi:10.1038/nature05925

Finch RA, Donoviel DB, Potter D, Shi M, Fan A, Freed DD, Wang C-Y, Zambrowicz BP, Ramirez-Solis R, Sands AT, Zhang N. 2002. mdmx is a negative regulator of p53 activity in vivo. *Cancer Res* **62**:3221–3225.

Funk JS, Klimovich M, Drangenstein D, Pielhoop O, Hunold P, Borowek A, Noeparast M, Pavlakis E, Neumann M, Balourdas D-I, Kochhan K, Merle N, Bullwinkel I, Wanzel M, Elmshäuser S, Teply-Szymanski J, Nist A, Procida T, Bartkuhn M, Humpert K, Mernberger M, Savai R, Soussi T, Joerger AC, Stiewe T. 2025. Deep CRISPR mutagenesis characterizes the functional diversity of TP53 mutations. *Nat Genet* **57**:140–153. doi:10.1038/s41588-024-02039-4

Gencel-Augusto J, Lozano G. 2020. p53 tetramerization: at the center of the dominant-negative effect of mutant p53. *Genes Dev* **34**:1128–1146. doi:10.1101/gad.340976.120

Gener-Ricos G, Bewersdorf JP, Loghavi S, Bataller A, Goldberg AD, Sasaki K, Famulare C, Takahashi K, Issa GC, Borthakur G, Kadia TM, Short NJ, Senapati J, Carter BZ, Patel KP, Kantarjian H, Andreeff M, Stein EM, DiNardo CD. 2024. *TP53* Y220C mutations in patients with myeloid malignancies. *Leukemia & Lymphoma* **65**:1511–1515. doi:10.1080/10428194.2024.2363440

Greten FR, Grivennikov SI. 2019. Inflammation and Cancer: Triggers, Mechanisms, and

Consequences. *Immunity* **51**:27–41. doi:10.1016/j.immuni.2019.06.025
Guimond MJ, Wang B, Fujita J, Terhorst C, Croy BA. 1996. Pregnancy-associated uterine granulated metrial gland cells in mutant and transgenic mice. *Am J Reprod Immunol* **35**:501–509. doi:10.1111/j.1600-0897.1996.tb00049.x
Hainaut P, Pfeifer GP. 2016. Somatic TP53 Mutations in the Era of Genome Sequencing. *Cold Spring Harb Perspect Med* **6**:a026179. doi:10.1101/cshperspect.a026179
Ham SW, Jeon H-Y, Jin X, Kim E-J, Kim J-K, Shin YJ, Lee Y, Kim SH, Lee SY, Seo S, Park MG, Kim H-M, Nam D-H, Kim H. 2019. TP53 gain-of-function mutation promotes inflammation in glioblastoma. *Cell Death Differ* **26**:409–425. doi:10.1038/s41418-018-0126-3
Hanahan D. 2022. Hallmarks of Cancer: New Dimensions. *Cancer Discovery* **12**:31–46. doi:10.1158/2159-8290.CD-21-1059
Hanel W, Marchenko N, Xu S, Yu SX, Weng W, Moll U. 2013. Two hot spot mutant p53 mouse models display differential gain of function in tumorigenesis. *Cell Death Differ* **20**:898–909. doi:10.1038/cdd.2013.17
Hollstein M, Sidransky D, Vogelstein B, Harris CC. 1991. p53 mutations in human cancers. *Science* **253**:49–53. doi:10.1126/science.1905840
Hu W. 2009. The role of p53 gene family in reproduction. *Cold Spring Harb Perspect Biol* **1**:a001073. doi:10.1101/cshperspect.a001073
Hu W, Feng Z, Teresky AK, Levine AJ. 2007. p53 regulates maternal reproduction through LIF. *Nature* **450**:721–724. doi:10.1038/nature05993
Humpton TJ, Hock AK, Maddocks ODK, Vousden KH. 2018. p53-mediated adaptation to serine starvation is retained by a common tumour-derived mutant. *Cancer Metab* **6**:18. doi:10.1186/s40170-018-0191-6
Iwakuma T, Parant JM, Fasulo M, Zwart E, Jacks T, de Vries A, Lozano G. 2004. Mutation at p53 serine 389 does not rescue the embryonic lethality in mdm2 or mdm4 null mice. *Oncogene* **23**:7644–7650. doi:10.1038/sj.onc.1207793
Jacks T, Remington L, Williams BO, Schmitt EM, Halachmi S, Bronson RT, Weinberg RA. 1994. Tumor spectrum analysis in p53-mutant mice. *Curr Biol* **4**:1–7. doi:10.1016/s0960-9822(00)00002-6
Joerger AC, Ang HC, Fersht AR. 2006. Structural basis for understanding oncogenic p53 mutations and designing rescue drugs. *Proc Natl Acad Sci U S A* **103**:15056–15061. doi:10.1073/pnas.0607286103
Jones SN, Roe AE, Donehower LA, Bradley A. 1995. Rescue of embryonic lethality in Mdm2-deficient mice by absence of p53. *Nature* **378**:206–208. doi:10.1038/378206a0
Kadosh E, Snir-Alkalay I, Venkatachalam A, May S, Lasry A, Elyada E, Zinger A, Shaham M, Vaalani G, Mernberger M, Stiewe T, Pikarsky E, Oren M, Ben-Neriah Y. 2020. The gut microbiome switches mutant p53 from tumour-suppressive to oncogenic. *Nature* **586**:133–138. doi:10.1038/s41586-020-2541-0
Karthik KV, Rajalingam A, Shivashankar M, Ganjiwale A. 2022. Recursive Feature Elimination-based Biomarker Identification for Open Neural Tube Defects. *Curr Genomics* **23**:195–206. doi:10.2174/1389202923666220511162038
Kastan MB, Zhan Q, el-Deiry WS, Carrier F, Jacks T, Walsh WV, Plunkett BS, Vogelstein B, Fornace AJ. 1992. A mammalian cell cycle checkpoint pathway utilizing p53 and GADD45 is defective in ataxia-telangiectasia. *Cell* **71**:587–597. doi:10.1016/0092-8674(92)90593-2
Kennedy MC, Lowe SW. 2022. Mutant p53: it's not all one and the same. *Cell Death Differ* **29**:983–987. doi:10.1038/s41418-022-00989-y

Kim E, Deppert W. 2007. Interactions of mutant p53 with DNA: guilt by association. *Oncogene* **26**:2185–2190. doi:10.1038/sj.onc.1210312

Kim MP, Lozano G. 2018. Mutant p53 partners in crime. *Cell Death Differ* **25**:161–168. doi:10.1038/cdd.2017.185

Kotler E, Shani O, Goldfeld G, Lotan-Pompan M, Tarcic O, Gershoni A, Hopf TA, Marks DS, Oren M, Segal E. 2018. A Systematic p53 Mutation Library Links Differential Functional Impact to Cancer Mutation Pattern and Evolutionary Conservation. *Mol Cell* **71**:178-190.e8. doi:10.1016/j.molcel.2018.06.012

Kroemer G, Pouyssegur J. 2008. Tumor Cell Metabolism: Cancer's Achilles' Heel. *Cancer Cell* **13**:472–482. doi:10.1016/j.ccr.2008.05.005

Lallemand Y, Luria V, Haffner-Krausz R, Lonai P. 1998. Maternally expressed PGK-Cre transgene as a tool for early and uniform activation of the Cre site-specific recombinase. *Transgenic Res* **7**:105–112. doi:10.1023/a:1008868325009

Lian Q, Dheen ST, Liao D, Tay SSW. 2004. Enhanced inflammatory response in neural tubes of embryos derived from diabetic mice exposed to a teratogen. *J of Neuroscience Research* **75**:554–564. doi:10.1002/jnr.20006

Liao Y, Smyth GK, Shi W. 2014. featureCounts: an efficient general purpose program for assigning sequence reads to genomic features. *Bioinformatics* **30**:923–930. doi:10.1093/bioinformatics/btt656

Liu J, Yang J, Pan Q, Wang Xiangyu, Wang Xinyin, Chen H, Zheng X, Huang Q. 2024. MDM4 was associated with poor prognosis and tumor-immune infiltration of cancers. *Eur J Med Res* **29**:79. doi:10.1186/s40001-024-01684-z

Love MI, Huber W, Anders S. 2014. Moderated estimation of fold change and dispersion for RNA-seq data with DESeq2. *Genome Biol* **15**:550. doi:10.1186/s13059-014-0550-8

Lowe SW, Schmitt EM, Smith SW, Osborne BA, Jacks T. 1993. p53 is required for radiation-induced apoptosis in mouse thymocytes. *Nature* **362**:847–849. doi:10.1038/362847a0

Marine J-C, Francoz S, Maetens M, Wahl G, Toledo F, Lozano G. 2006. Keeping p53 in check: essential and synergistic functions of Mdm2 and Mdm4. *Cell Death Differ* **13**:927–934. doi:10.1038/sj.cdd.4401912

McCann JJ, Vasilevskaya IA, McNair C, Gallagher P, Neupane NP, De Leeuw R, Shafi AA, Dylgjeri E, Mandigo AC, Schiewer MJ, Knudsen KE. 2022. Mutant p53 elicits context-dependent pro-tumorigenic phenotypes. *Oncogene* **41**:444–458. doi:10.1038/s41388-021-01903-5

McNairn AJ, Chuang C-H, Bloom JC, Wallace MD, Schimenti JC. 2019. Female-biased embryonic death from inflammation induced by genomic instability. *Nature* **567**:105–108. doi:10.1038/s41586-019-0936-6

Migliorini D, Lazzerini Denchi E, Danovi D, Jochemsen A, Capillo M, Gobbi A, Helin K, Pelicci PG, Marine J-C. 2002. Mdm4 (Mdmx) regulates p53-induced growth arrest and neuronal cell death during early embryonic mouse development. *Mol Cell Biol* **22**:5527–5538. doi:10.1128/MCB.22.15.5527-5538.2002

Montes de Oca Luna R, Wagner DS, Lozano G. 1995. Rescue of early embryonic lethality in mdm2-deficient mice by deletion of p53. *Nature* **378**:203–206. doi:10.1038/378203a0

Morselli E, Tasdemir E, Maiuri MC, Galluzzi L, Kepp O, Criollo A, Vicencio JM, Soussi T, Kroemer G. 2008. Mutant p53 protein localized in the cytoplasm inhibits autophagy. *Cell Cycle* **7**:3056–3061. doi:10.4161/cc.7.19.6751

Pal A, Gonzalez-Malerva L, Eaton S, Xu C, Zhang Y, Grief D, Sakala L, Nwekwo L, Zeng J,

Christensen G, Gupta C, Streitwieser E, Singharoy A, Park JG, LaBaer J. 2023. Multidimensional quantitative phenotypic and molecular analysis reveals neomorphic behaviors of p53 missense mutants. *NPJ Breast Cancer* **9**:78. doi:10.1038/s41523-023-00582-7

Parant J, Chavez-Reyes A, Little NA, Yan W, Reinke V, Jochemsen AG, Lozano G. 2001. Rescue of embryonic lethality in Mdm4-null mice by loss of Trp53 suggests a nonoverlapping pathway with MDM2 to regulate p53. *Nat Genet* **29**:92–95. doi:10.1038/ng714

Pfister NT, Prives C. 2017. Transcriptional Regulation by Wild-Type and Cancer-Related Mutant Forms of p53. *Cold Spring Harb Perspect Med* **7**:a026054. doi:10.1101/cshperspect.a026054

Rakotopare J, Lejour V, Duval C, Eldawra E, Escoffier H, Toledo F. 2023. A systematic approach identifies p53-DREAM pathway target genes associated with blood or brain abnormalities. *Dis Model Mech* **16**:dmm050376. doi:10.1242/dmm.050376

Rakotopare J, Toledo F. 2023. p53 in the Molecular Circuitry of Bone Marrow Failure Syndromes. *Int J Mol Sci* **24**:14940. doi:10.3390/ijms241914940

Rambold AS, Lippincott-Schwartz J. 2011. Mechanisms of mitochondria and autophagy crosstalk. *Cell Cycle* **10**:4032–4038. doi:10.4161/cc.10.23.18384

Regeling A, Armata HL, Gallant J, Jones SN, Sluss HK. 2011. Mice defective in p53 nuclear localization signal 1 exhibit exencephaly. *Transgenic Res* **20**:899–912. doi:10.1007/s11248-010-9468-4

Rockwell NC, Yang W, Warrington NM, Staller MV, Griffith M, Griffith OL, Gurnett CA, Cohen BA, Baldridge D, Rubin JB. 2021. Sex- and Mutation-Specific p53 Gain-of-Function Activity in Gliomagenesis. *Cancer Research Communications* **1**:148–163. doi:10.1158/2767-9764.CRC-21-0026

Rodier F, Coppé J-P, Patil CK, Hoeijmakers WAM, Muñoz DP, Raza SR, Freund A, Campeau E, Davalos AR, Campisi J. 2009. Persistent DNA damage signalling triggers senescence-associated inflammatory cytokine secretion. *Nat Cell Biol* **11**:973–979. doi:10.1038/ncb1909

Sah VP, Attardi LD, Mulligan GJ, Williams BO, Bronson RT, Jacks T. 1995. A subset of p53-deficient embryos exhibit exencephaly. *Nat Genet* **10**:175–180. doi:10.1038/ng0695-175

Shirole N, Pal D, Kastenhuber E, Senturk S, Boroda J, Pisterzi P, Miller M, Munoz G, Anderluh M, Ladanyi M, Lowe S, Sordella R. 2016. TP53 exon-6 truncating mutations produce separation of function isoforms with pro-tumorigenic functions. *Elife* e17929. doi:doi: 10.7554/eLife.17929

Simeonova I, Jaber S, Draskovic I, Bardot B, Fang M, Bouarich-Bourimi R, Lejour V, Charbonnier L, Soudais C, Bourdon J-C, Huerre M, Londono-Vallejo A, Toledo F. 2013. Mutant mice lacking the p53 C-terminal domain model telomere syndromes. *Cell Rep* **3**:2046–2058. doi:10.1016/j.celrep.2013.05.028

Simeonova I, Lejour V, Bardot B, Bouarich-Bourimi R, Morin A, Fang M, Charbonnier L, Toledo F. 2012. Fuzzy Tandem Repeats Containing p53 Response Elements May Define Species-Specific p53 Target Genes. *PLoS Genet* **8**:e1002731. doi:10.1371/journal.pgen.1002731

Sionov RV, Vlahopoulos SA, Granot Z. 2015. Regulation of Bim in Health and Disease. *Oncotarget* **6**:23058–23134. doi:10.18632/oncotarget.5492

Solier S, Müller S, Cañeque T, Versini A, Mansart A, Sindikubwabo F, Baron L, Emam L, Gestraud P, Pantoș GD, Gandon V, Gaillet C, Wu T-D, Dingli F, Loew D, Baulande S, Durand S, Sencio V, Robil C, Trottein F, Péricat D, Näser E, Cougoule C, Meunier E, Bègue A-L, Salmon H, Manel N, Puisieux A, Watson S, Dawson MA, Servant N, Kroemer G, Annane D, Rodriguez R. 2023. A druggable copper-signalling pathway that drives inflammation. *Nature*

617:386–394. doi:10.1038/s41586-023-06017-4
Stein Y, Aloni-Grinstein R, Rotter V. 2020. Mutant p53 oncogenicity: dominant-negative or gain-of-function? *Carcinogenesis* **41**:1635–1647. doi:10.1093/carcin/bgaa117
Subramanian A, Tamayo P, Mootha VK, Mukherjee S, Ebert BL, Gillette MA, Paulovich A, Pomeroy SL, Golub TR, Lander ES, Mesirov JP. 2005. Gene set enrichment analysis: A knowledge-based approach for interpreting genome-wide expression profiles. *Proc Natl Acad Sci USA* **102**:15545–15550. doi:10.1073/pnas.0506580102
Tateossian H, Morse S, Simon MM, Dean CH, Brown SDM. 2015. Interactions between the otitis media gene, *Fbxo11* , and *p53* in the mouse embryonic lung. *Disease Models & Mechanisms* dmm.022426. doi:10.1242/dmm.022426
Taylor AW, Ng TF. 2018. Negative regulators that mediate ocular immune privilege. *J Leukoc Biol*. doi:10.1002/JLB.3MIR0817-337R
Toledo F, Krummel KA, Lee CJ, Liu C-W, Rodewald L-W, Tang M, Wahl GM. 2006. A mouse p53 mutant lacking the proline-rich domain rescues Mdm4 deficiency and provides insight into the Mdm2-Mdm4-p53 regulatory network. *Cancer Cell* **9**:273–285. doi:10.1016/j.ccr.2006.03.014
Tseng T-H, Wang C-J, Lee Y-J, Shao Y-C, Shen C-H, Lee K-C, Tung S-Y, Kuo H-C. 2022. Suppression of the Proliferation of Huh7 Hepatoma Cells Involving the Downregulation of Mutant p53 Protein and Inactivation of the STAT 3 Pathway with Ailanthoidol. *Int J Mol Sci* **23**:5102. doi:10.3390/ijms23095102
Varner MW, Costantine MM, Jablonski KA, Rouse DJ, Mercer BM, Leveno KJ, Reddy UM, Buhimschi C, Wapner RJ, Sorokin Y, Thorp JM, Ramin SM, Malone FD, Carpenter M, O'sullivan MJ, Peaceman AM, Dudley DJ, Caritis SN, Eunice Kennedy Shriver National Institute of Child Health and Human Development Maternal-Fetal Medicine Units Network. 2020. Sex-Specific Genetic Susceptibility to Adverse Neurodevelopmental Outcome in Offspring of Pregnancies at Risk of Early Preterm Delivery. *Am J Perinatol* **37**:281–290. doi:10.1055/s-0039-1678535
Vassilev LT, Vu BT, Graves B, Carvajal D, Podlaski F, Filipovic Z, Kong N, Kammlott U, Lukacs C, Klein C, Fotouhi N, Liu EA. 2004. In vivo activation of the p53 pathway by small-molecule antagonists of MDM2. *Science* **303**:844–848. doi:10.1126/science.1092472
Ventura A, Kirsch DG, McLaughlin ME, Tuveson DA, Grimm J, Lintault L, Newman J, Reczek EE, Weissleder R, Jacks T. 2007. Restoration of p53 function leads to tumour regression in vivo. *Nature* **445**:661–665. doi:10.1038/nature05541
Vikhanskaya F, Lee MK, Mazzoletti M, Broggini M, Sabapathy K. 2007. Cancer-derived p53 mutants suppress p53-target gene expression--potential mechanism for gain of function of mutant p53. *Nucleic Acids Res* **35**:2093–2104. doi:10.1093/nar/gkm099
Voskarides K, Giannopoulou N. 2023. The Role of TP53 in Adaptation and Evolution. *Cells* **12**:512. doi:10.3390/cells12030512
Vousden KH, Lane DP. 2007. p53 in health and disease. *Nat Rev Mol Cell Biol* **8**:275–283. doi:10.1038/nrm2147
Wang Z, Burigotto M, Ghetti S, Vaillant F, Tan T, Capaldo B, Palmieri M, Hirokawa Y, Tai L, Simpson D, Chang C, Huang A, Lieschke E, Diepstraten S, Kaloni D, Riffkin C, Huang D, Li Wai Suen C, Garnham A, Gibbs P, Visvader J, Sieber O, Herold M, Fava L, Kelly G, Strasser A. 2023. Loss-of-function but not gain-of-function properties of mutant TP53 are critical for the proliferation, survival and metastasis of a broad range of cancer cells. *Cancer Discov*. doi:10.1158/2159-8290.CD-23-0402.

Xiong S, Chachad D, Zhang Y, Gencel-Augusto J, Sirito M, Pant V, Yang P, Sun C, Chau G, Qi Y, Su X, Whitley EM, El-Naggar AK, Lozano G. 2022. Differential Gain-of-Function Activity of Three p53 Hotspot Mutants *In Vivo*. *Cancer Research* **82**:1926–1936. doi:10.1158/0008-5472.CAN-21-3376

Xu J, Qian J, Hu Y, Wang J, Zhou X, Chen H, Fang J-Y. 2014. Heterogeneity of Li-Fraumeni Syndrome links to unequal gain-of-function effects of p53 mutations. *Sci Rep* **4**:4223. doi:10.1038/srep04223

Ye J, Tong Y, Lv J, Peng R, Chen S, Kuang L, Su K, Zheng Y, Zhang T, Zhang F, Jin L, Yang X, Wang H. 2020. Rare mutations in the autophagy-regulating gene AMBRA1 contribute to human neural tube defects. *Hum Mutat* **41**:1383–1393. doi:10.1002/humu.24028

Zhang X, Wei H. 2021. Role of Decidual Natural Killer Cells in Human Pregnancy and Related Pregnancy Complications. *Front Immunol* **12**:728291. doi:10.3389/fimmu.2021.728291

Zhao J, Tian Y, Zhang H, Qu L, Chen Y, Liu Q, Luo Y, Wu X. 2019. p53 Mutant p53 ^{N236S} Induces Neural Tube Defects in Female Embryos. *Int J Biol Sci* **15**:2006–2015. doi:10.7150/ijbs.31451

Zhao M, Chen Y-H, Dong X-T, Zhou J, Chen X, Wang H, Wu S-X, Xia M-Z, Zhang C, Xu D-X. 2013. Folic Acid Protects against Lipopolysaccharide-Induced Preterm Delivery and Intrauterine Growth Restriction through Its Anti-Inflammatory Effect in Mice. *PLoS ONE* **8**:e82713. doi:10.1371/journal.pone.0082713

Zhao M, Wang T, Gleber-Netto FO, Chen Z, McGrail DJ, Gomez JA, Ju W, Gadhikar MA, Ma W, Shen L, Wang Q, Tang X, Pathak S, Raso MG, Burks JK, Lin S-Y, Wang J, Multani AS, Pickering CR, Chen J, Myers JN, Zhou G. 2024. Mutant p53 gains oncogenic functions through a chromosomal instability-induced cytosolic DNA response. *Nat Commun* **15**:180. doi:10.1038/s41467-023-44239-2

Zhou J, Luo J, Li Peiwei, Zhou Y, Li Peichao, Wang F, Mallio CA, Rossi G, Jalal AH, Filipovic N, Tian Z, Zhao X. 2022. Triptolide promotes degradation of the unfolded gain-of-function Tp53R175H/Y220C mutant protein by initiating heat shock protein 70 transcription in non-small cell lung cancer. *Transl Lung Cancer Res* **11**:802–816. doi:10.21037/tlcr-22-312

Figures

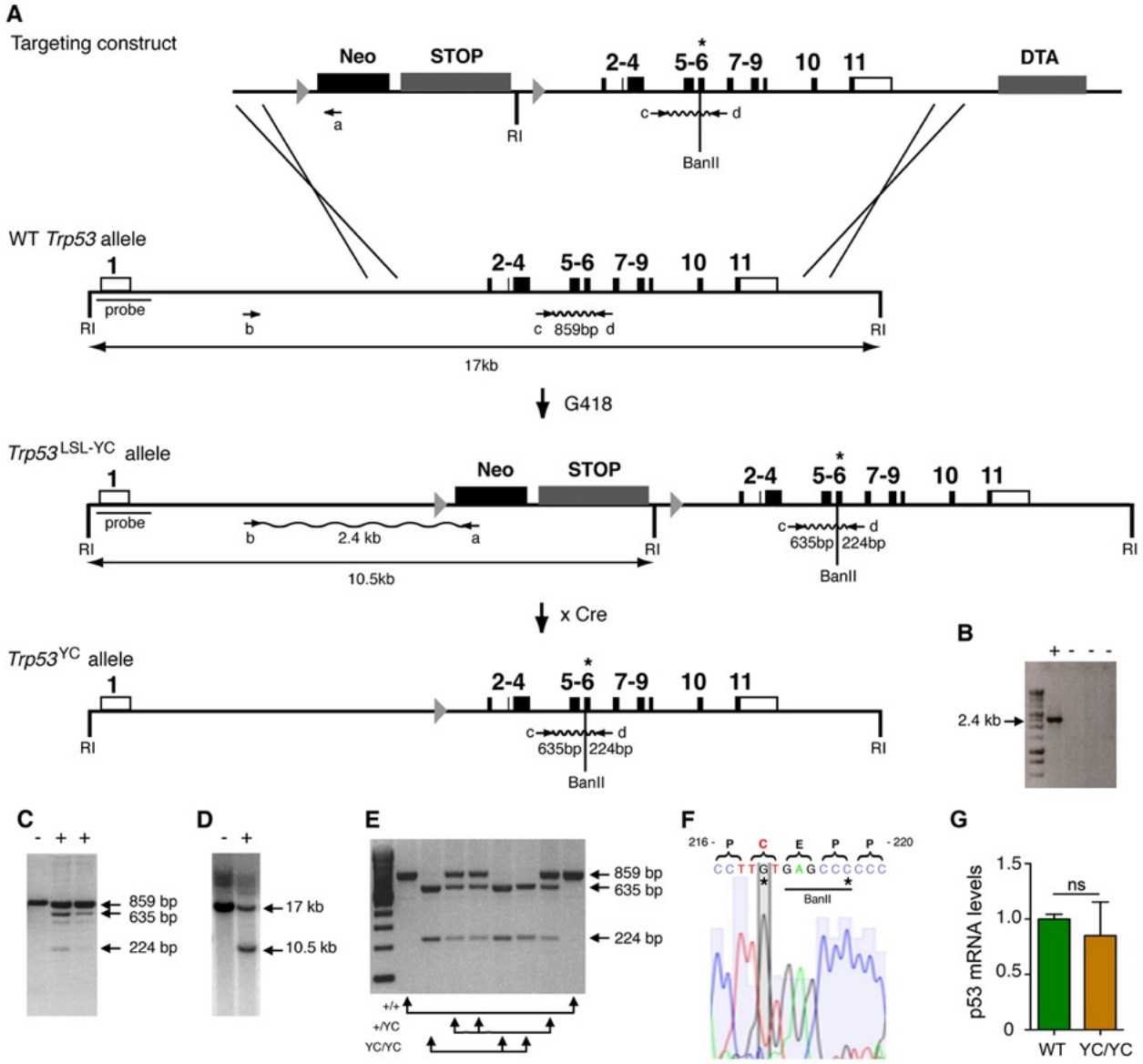

Figure 1. Targeting the Y217C missense mutation at the mouse *Trp53* locus.
(A) Targeting strategy. The wildtype (WT) *Trp53* gene is within a 17 kb-long EcoRI (RI) fragment (black boxes are for coding sequences and white boxes for UTRs). The targeting construct contains: (1) a 1.5 kb-long 5' homology region; (2) a Lox-Stop-Lox (LSL) cassette with a *neomycin* selection gene (Neo), four transcriptional stops (STOP) and an EcoRI site, flanked by LoxP sites (arrowheads); (3) p53 coding exons, including the Y217C (YC) missense mutation in exon 6 (asterisk) and an additional BanII site; (4) a 2.8 kb-long 3' homology region; and (5) the diphteria α-toxin (DTA) gene for targeting enrichment. Proper recombinants with a *Trp53*$^{\text{LSL-Y217C}}$ allele, resulting from the described crossing-overs, were G418 resistant. They were identified by a 2.4 kb-long band after PCR with primers a and b, and confirmed by bands of 635 and 224 bp after PCR with primers c and d and BanII digestion. They were also verified by Southern blot with

the indicated probe as containing a 10.5 kb EcoRI band. Two recombinant ES clones were injected into blastocysts to generate chimeras, and germline transmission was verified by genotyping with primers c and d and BanII digestion. Excision of the LSL cassette was performed *in vivo*, by breeding *Trp53*$^{+/LSL\text{-}Y217C}$ male mice with females carrying the PGK-*Cre* transgene, to obtain mice with a *Trp53*^{Y217C} allele. **(B-D)** Screening of recombinant ES clones (+) by PCR with primers a and b (B); PCR with primers c and d then BanII digestion (C); Southern blot (D). **(E)** Genotyping of mouse embryonic fibroblasts (MEFs) from an intercross of *Trp53*$^{+/Y217C}$ mice, by PCR with primers c and d and BanII digestion. **(F)** *Trp53*^{Y217C} sequence around codon 217. The introduced Y217C missense mutation and the silent mutation creating an additional BanII restriction site are highlighted (asterisks). **(G)** WT and *Trp53*$^{Y217C/Y217C}$ (YC/YC) MEFs express similar p53 mRNA levels. Total RNA was extracted, then p53 mRNAs were quantified by real-time qPCR, normalized to control mRNAs and the amount in WT cells was assigned the value of 1. Primer sequences are listed in Table S8.

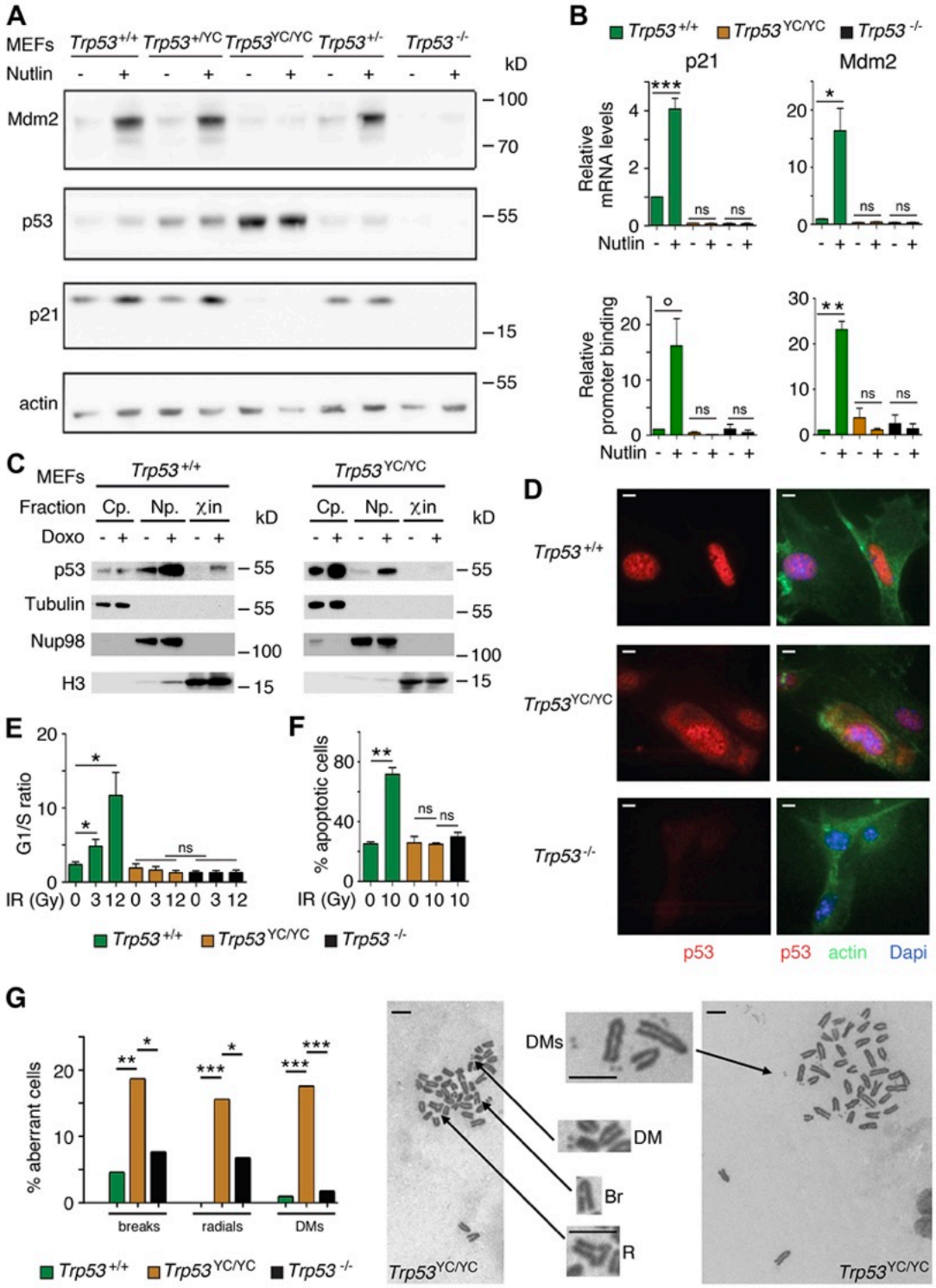

Figure 2. *Trp53*$^{Y217C/Y217C}$ cells exhibit alterations in p53 abundance and subcellular localization, defective responses to DNA damage, and increased chromosomal instability. **(A)** Increased p53 protein levels in *Trp53*$^{Y217C/Y217C}$ and *Trp53*$^{+/Y217C}$ MEFs. MEFs of the indicated genotypes were treated or not with 10 µM Nutlin 3a for 24 h, then protein extracts were immunoblotted with antibodies against Mdm2, p53, p21 and actin. **(B)** The transactivation of classical p53 target genes *Cdkn1a/p21* and *Mdm2* is impaired in *Trp53*$^{Y217C/Y217C}$ cells. WT,

Trp53$^{Y217C/Y217C}$ and *Trp53*$^{-/-}$ MEFs were treated as in (A), then (top) mRNAs were quantified in 5-6 independent experiments using real-time PCR, with results normalized to control mRNAs and mean RNA amounts in unstressed WT cells assigned a value of 1; or (bottom) ChIP assays were performed at the *Cdkn1a* and *Mdm2* promoters in 2-3 independent experiments with an antibody against p53 or rabbit IgG as a negative control. Immunoprecipitates were quantified using real-time PCR, normalized to data over an irrelevant region, and the amount in unstressed WT cells was assigned a value of 1. **(C)** Assessment of p53^{WT} and p53^{Y217C} subcellular localization by cellular fractionation. WT and *Trp53*$^{Y217C/Y217C}$ MEFs were treated or not with 1 µM doxorubicin (Doxo) for 24 hr, submitted to cellular fractionation, then protein extracts were immunoblotted with antibodies against p53 or the fraction controls Tubulin for cytoplasm (Cp.), Nup98 for nucleoplasm (Np.) and histone H3 for chromatin (χin). **(D)** Assessment of p53^{WT} and p53^{Y217C} subcellular localization by immunofluorescence. WT, *Trp53*$^{Y217C/Y217C}$ and *Trp53*$^{-/-}$ MEFs were treated with 10 µM Nutlin 3a for 24 h, then stained with antibodies against p53 (red) or actin (green) and DNA was counterstained with DAPI (blue). **(E)** Absence of a cell cycle arrest response in *Trp53*$^{Y217C/Y217C}$ MEFs. Asynchronous cell populations of *Trp53*$^{+/+}$, *Trp53*$^{Y217C/Y217C}$ and *Trp53*$^{-/-}$ MEFs were analyzed 24 hr after 0, 3 or 12 Gy ɣ-irradiation. Results from 3 independent experiments. **(F)** Absence of a p53-dependent apoptotic response in *Trp53*$^{Y217C/Y217C}$ thymocytes. Age-matched mice of the indicated genotypes were left untreated or submitted to 10 Gy whole-body ɣ-irradiation then sacrificed after 4 hr and their thymocytes were stained with Annexin V-FITC and analyzed by FACS, in 2 independent experiments. **(G)** Increased chromosomal instability in *Trp53*$^{Y217C/Y217C}$ fibroblasts. Metaphase spreads were prepared from WT, *Trp53*$^{Y217C/Y217C}$ and *Trp53*$^{-/-}$ MEFs at passage 4, then aberrant metaphases (with chromosome breaks, radial chromosomes or DMs) were scored. Left: distribution of aberrant metaphases. Data from 110 WT, 97 *Trp53*$^{Y217C/Y217C}$ or 119 *Trp53*$^{-/-}$ complete diploid metaphases, independently observed by two experimenters. Right: examples of two aberrant *Trp53*$^{Y217C/Y217C}$ metaphases: one with a double minute chromosome (DM), a chromosome break (Br) and a radial chromosome (R), the other with multiple DMs. Enlargements of regions of interest are presented between the two metaphases. Scale bars (D, G): 5 µm. ***P<0.001, **P<0.01, *P<0.05, °P=0.09, ns: non-significant by Student's t (B, E, F) or Fischer's (G) tests.

A

at weaning

Trp53$^{+/-}$ x *Trp53*$^{+/-}$	Nbr. females obs (exp)	Nbr. males obs (exp)	Sex ratio (f/m)	Total
Trp53$^{+/+}$	24 (25)	20 (25)	1.2	196
Trp53$^{+/-}$	59 (49)	57 (49)	1.04	
Trp53$^{-/-}$	8 (25)	28 (25)	0.29	

Trp53$^{+/YC}$ x *Trp53*$^{+/YC}$	Nbr. females obs (exp)	Nbr. males obs (exp)	Sex ratio (f/m)	Total
Trp53$^{+/+}$	80 (85)	88 (85)	0.91	677
Trp53$^{+/YC}$	209 (169)	221 (169)	0.95	
Trp53$^{YC/YC}$	4 (85)	75 (85)	0.05	

B

E12.5-E16.5 embryos

Trp53$^{+/YC}$ x *Trp53*$^{+/YC}$ or *Trp53*$^{+/YC}$ x *Trp53*$^{YC/YC}$	Nbr. females	f exenc. (o.a.)	Nbr. males	m exenc. (o.a.)	Sex ratio (f/m)	Total
Trp53$^{+/+}$	12	0 (0)	14	0 (0)	0.86	169
Trp53$^{+/YC}$	47	0 (0)	48	0 (0)	0.98	
Trp53$^{YC/YC}$	26	10 (1)	22	0 (0)	1.18	

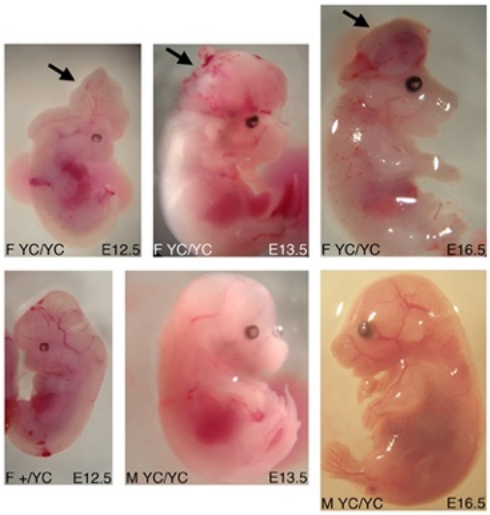

C

at birth

Trp53$^{+/YC}$ x *Trp53*$^{+/YC}$ or *Trp53*$^{+/YC}$ x *Trp53*$^{YC/YC}$	Nbr. females	Nbr. males	Sex ratio (f/m)	Total
Trp53$^{+/+}$	20	18	1.11	162
Trp53$^{+/YC}$	50	47	1.06	
Trp53$^{YC/YC}$	5	22	0.23	

Figure 3. *Trp53*$^{Y217C/Y217C}$ mice exhibit female-specific perinatal lethality.

(A) Distribution of weaned mice obtained from *Trp53*$^{+/-}$ or *Trp53*$^{+/Y217C}$ intercrosses. Obs: observed numbers of mice at weaning (P21); exp: expected numbers assuming a Mendelian distribution without sex distortion; f/m: observed female/male ratios. Consistent with previous reports, the observed distribution of weaned mice from *Trp53*$^{+/-}$ intercrosses did not conform to values expected for a Mendelian distribution without sex distortion (υ=5; χ^2=16.31>15.09), indicating a significant deficit in female *Trp53*$^{-/-}$ mice (top). The distribution of weaned mice from *Trp53*$^{+/Y217C}$ intercrosses diverged even more from values for a Mendelian distribution without sex

distortion (υ =5; χ^2=104.23>15.09), due to a striking deficit in female *Trp53*$^{Y217C/Y217C}$ mice (bottom). Differences between the frequencies of *Trp53*$^{Y217C/Y217C}$ (4/677) and *Trp53*$^{-/-}$ (8/196) females in the progeny, or between the female to male ratios for *Trp53*$^{Y217C/Y217C}$ (4/75) and *Trp53*$^{-/-}$ (8/28) animals, are statistically significant (P=0.0012 and P=0.0087 in Fischer's tests, respectively). **(B)** Exencephaly is frequently observed in p53$^{Y217C/Y217C}$ female embryos. Top: the distribution of E12.5-16.5 embryos from heterozygous (*Trp53*$^{+/Y217C}$) intercrosses or heterozygous-homozygous (*Trp53*$^{+/Y217C}$ x *Trp53*$^{Y217C/Y217C}$) crosses is shown. f or m exenc.: number of female or male embryos with exencephaly; o.a.: embryos with other abnormalities. Below, examples of female *Trp53*$^{Y217C/Y217C}$ embryos at E12.5, 13.5 and 16.5 exhibiting exencephaly (arrows) are each shown (center) together with a normal embryo from the same litter (bottom). **(C)** Distribution of mice at birth from the indicated crosses. Of note, out of five *Trp53*$^{Y217C/Y217C}$ females observed at birth, only one remained alive at weaning age. Thus, the female/male ratio for weaned *Trp53*$^{Y217C/Y217C}$ animals from these crosses was 1/22, a ratio similar to the one observed in A (4/75).

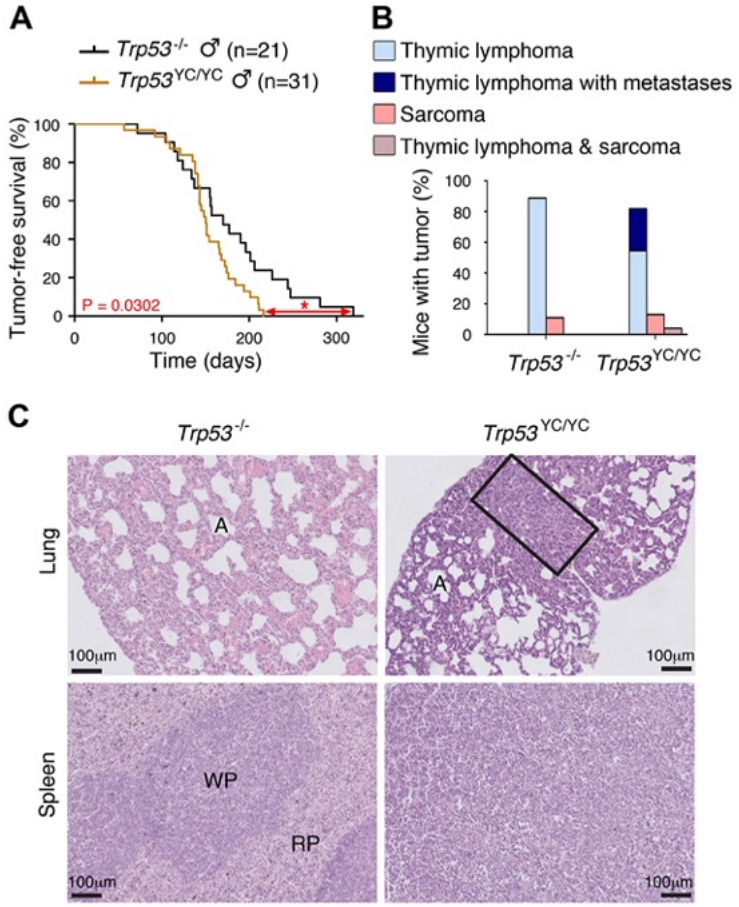

Figure 4. Oncogenic effects of the mutant protein in *Trp53*$^{Y217C/Y217C}$ male mice.
(A-B) In homozygous males, p53^{Y217C} leads to accelerated tumor-induced death (A), and aggressive metastatic tumors (B); n=cohort size. **(C)** Hematoxylin and eosin (H&E) staining of sections from the lung (top) and spleen (bottom) of *Trp53*$^{-/-}$ and *Trp53*$^{Y217C/Y217C}$ male mice, showing metastases in *Trp53*$^{Y217C/Y217C}$ animals. Normal organ structures are shown, with "A" indicating pulmonary alveoli, and "WP" and "RP" standing for splenic white and red pulp, respectively. In the lung section of the *Trp53*$^{Y217C/Y217C}$ mouse, the rectangle indicates a lymphoma area. In the spleen section of the *Trp53*$^{Y217C/Y217C}$ mouse, the typical splenic structures are absent due to massive tissue homogenization of the spleen by lymphoma cells.

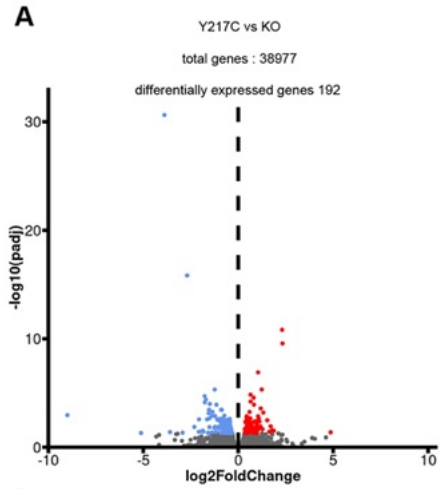

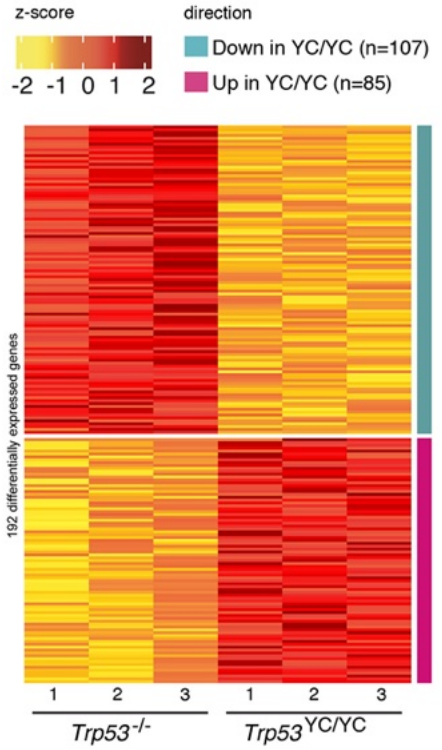

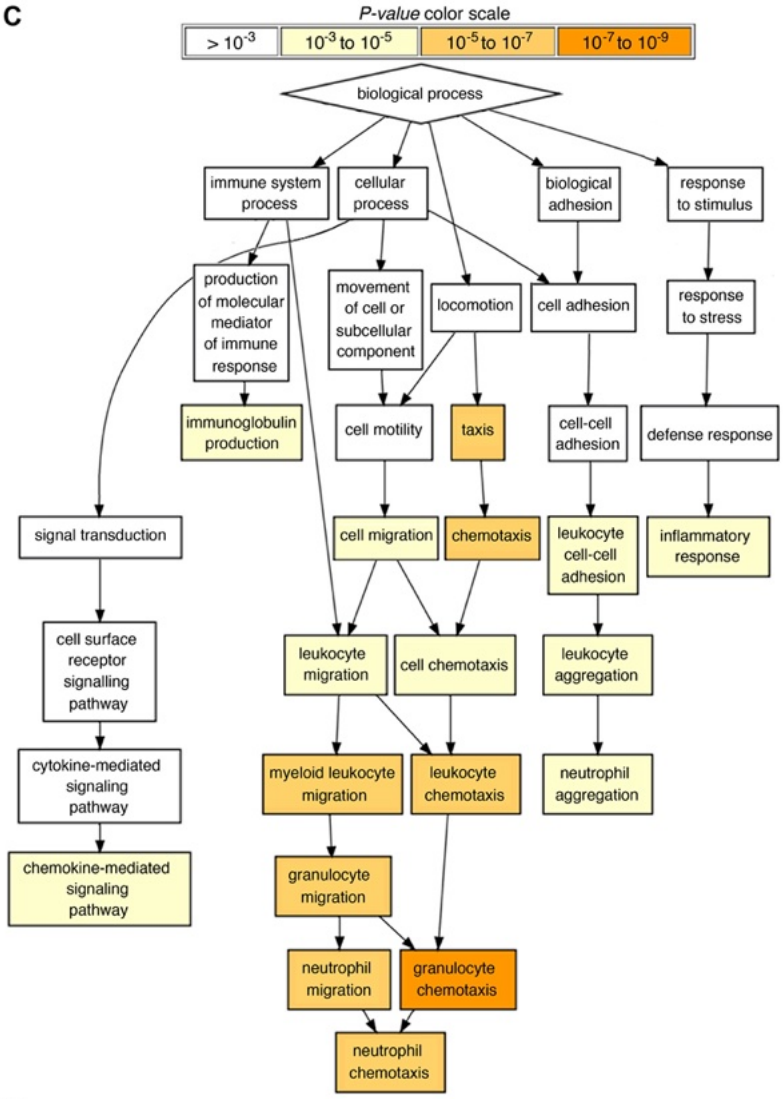

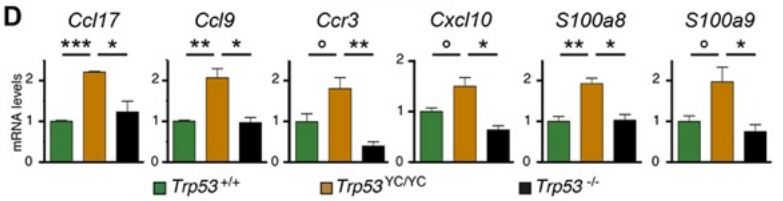

E

NAME	NES	NOM p-val	FDR q-val
WP_ELECTRON_TRANSPORT_CHAIN	2.3558052	0.0	0.0
REACTOME_ANTIMICROBIAL_PEPTIDES	2.2443378	0.0	0.0
REACTOME_TRANSLATION	2.2320845	0.0	0.0
REACTOME_RESPIRATORY_ELECTRON_TRANSPORT_ATP_SYNTHESIS_BY_CHEMIOSMOTIC _COUPLING_AND_HEAT_PRODUCTION_BY_UNCOUPLING_PROTEINS	2.1794727	0.0	4.955357E-4
REACTOME_MITOCHONDRIAL_TRANSLATION	2.1783278	0.0	3.9642857E-4
REACTOME_DEPOSITION_OF_NEW_CENPA_CONTAINING_NUCLEOSOMES_AT_THE_CENTROMERE	2.1476152	0.0	0.0016925472
REACTOME_RMTS_METHYLATE_HISTONE_ARGININES	2.1314094	0.0	0.00187209
REACTOME_RESPIRATORY_ELECTRON_TRANSPORT	2.1104455	0.0	0.0021443255
REACTOME_PRC2_METHYLATES_HISTONES_AND_DNA	2.103474	0.0	0.0021457656
REACTOME_CHEMOKINE_RECEPTORS_BIND_CHEMOKINES	2.0778365	0.0	0.0028372295
REACTOME_DEFENSINS	2.0432084	0.0	0.0038559462
REACTOME_EUKARYOTIC_TRANSLATION_INITIATION	2.0400345	0.0	0.0036215642
WP_OXIDATIVE_PHOSPHORYLATION	2.0248396	0.0	0.0049684355

F

NAME	NES	NOM p-val	FDR q-val
REACTOME_DECTIN_1_MEDIATED_NONCANONICAL_NF_KB_SIGNALING	1.9645858	0.0	0.00912268
REACTOME_ACTIVATION_OF_NF_KAPPAB_IN_B_CELLS	1.5596361	0.013550135	0.11355738
REACTOME_TNFR2_NON_CANONICAL_NF_KB_PATHWAY	1.400518	0.0149700595	0.21772017

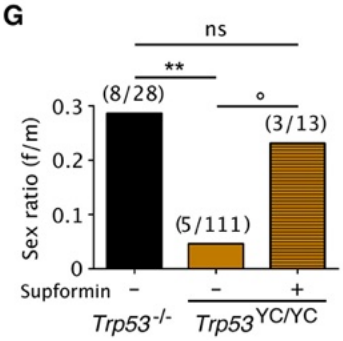

Figure 5. Evidence of inflammation in *Trp53*$^{Y217C/Y217C}$ mice.

(A-B) RNAseq analysis of thymi from *Trp53*$^{Y217C/Y217C}$ (n=3) and *Trp53*$^{-/-}$ (n=3) 8 weeks-old male mice. Volcano plot (A), with differentially expressed genes (DEGs), downregulated (blue) or upregulated (red) in *Trp53*$^{Y217C/Y217C}$ cells. Unsupervised clustering heat-map plot (B), with 192 DEGs ranked according to log_2 fold changes. **(C)** Gene Ontology (GO) analysis of DEGs. Out of 192 DEGs, 141 are associated with at least one GO term, according to the Gene Ontology enRIchment anaLysis and visuaLizAtion tool (GOrilla). For each GO term, enrichment was calculated by comparing with the full list of 19759 genes associated with a GO term, and results are presented here with a color scale according to P-value of enrichment. This analysis mainly revealed an enrichment for genes associated with white blood cell chemotaxis/migration and inflammation, as shown here. Complete results of the analysis are presented in Figure S11. **(D)** RT-qPCR analysis of the indicated genes in thymi from 8 weeks-old *Trp53*$^{+/+}$, *Trp53*$^{Y217C/Y217C}$ and *Trp53*$^{-/-}$ male mice. Means + s.e.m. (n=3 per genotype). ***P<0.001, **P<0.01, *P<0.05, °P<0.075 by Student's t test. **(E)** Gene set enrichment analysis (GSEA) of transcriptomes from *Trp53*$^{Y217C/Y217C}$ and *Trp53*$^{-/-}$ thymic cells. GSEA identified 13 gene sets enriched in *Trp53*$^{Y217C/Y217C}$ cells with normalized enrichment scores (NES) > 2. Nominal p-values (NOM p-val) and false discovery rate q-values (FDR q-val) are indicated. **(F)** GSEA provides evidence of increased NC-NF-kB signaling in *Trp53*$^{Y217C/Y217C}$ male thymocytes. Results are presented as in E. **(G)** Supformin (LCC-12), an anti-inflammatory molecule, increases the female to male ratio in *Trp53*$^{Y217C/Y217C}$ weaned pups. *Trp53*$^{+/Y217C}$ females were mated with *Trp53*$^{Y217C/Y217C}$ males, then oral gavage of pregnant females with 5 mg/kg supformin was performed on the 10th and 11th days post-coitum, and their progeny was genotyped at weaning. The female to male (f/m) ratio for *Trp53*$^{Y217C/Y217C}$ weaned pups that were exposed to supformin *in utero* (+) was compared to the f/m ratios for *Trp53*$^{-/-}$ or *Trp53*$^{Y217C/Y217C}$ weaned pups never exposed to supformin (-). Exposure to supformin led to a five-fold increase in the proportion of *Trp53*$^{Y217C/Y217C}$ weaned females. **P<0.01, °P=0.056, ns: non-significant by Fischer's test.

Supplemental Figures

Mouse 208-**T F R H S V V V P Y E P P E** A **G S** E Y **T T**- 228

Human 211-**T F R H S V V V P Y E P P E** V **G S** D C **T T**- 231

Figure S1. Protein sequence alignment showing homology between mouse p53 Tyrosine 217 and human p53 Tyrosine 220.
Portions of the DNA binding domains from the mouse (residues 208-228) and human (residues 211-231) p53 proteins are shown, with identical residues in bold, and mouse Tyrosine 217 and human Tyrosine 220 in red.

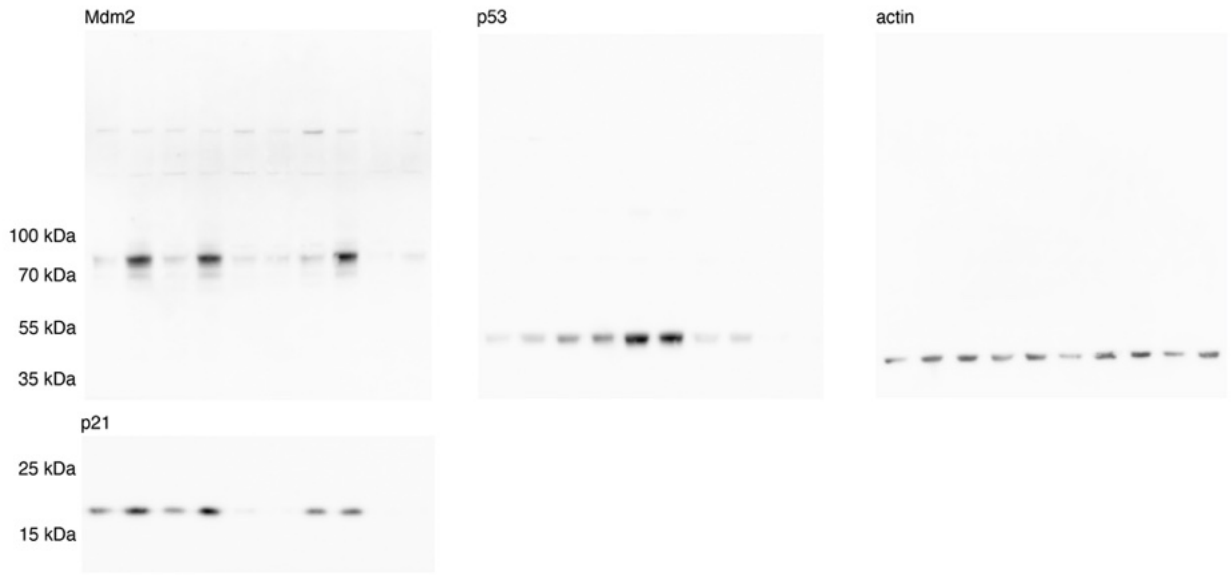

Figure S2. Uncropped images of the western blot presented in Figure 2A.
All images are from the same blot, cut in two below the 35 kDa marker before incubation with the indicated antibodies.

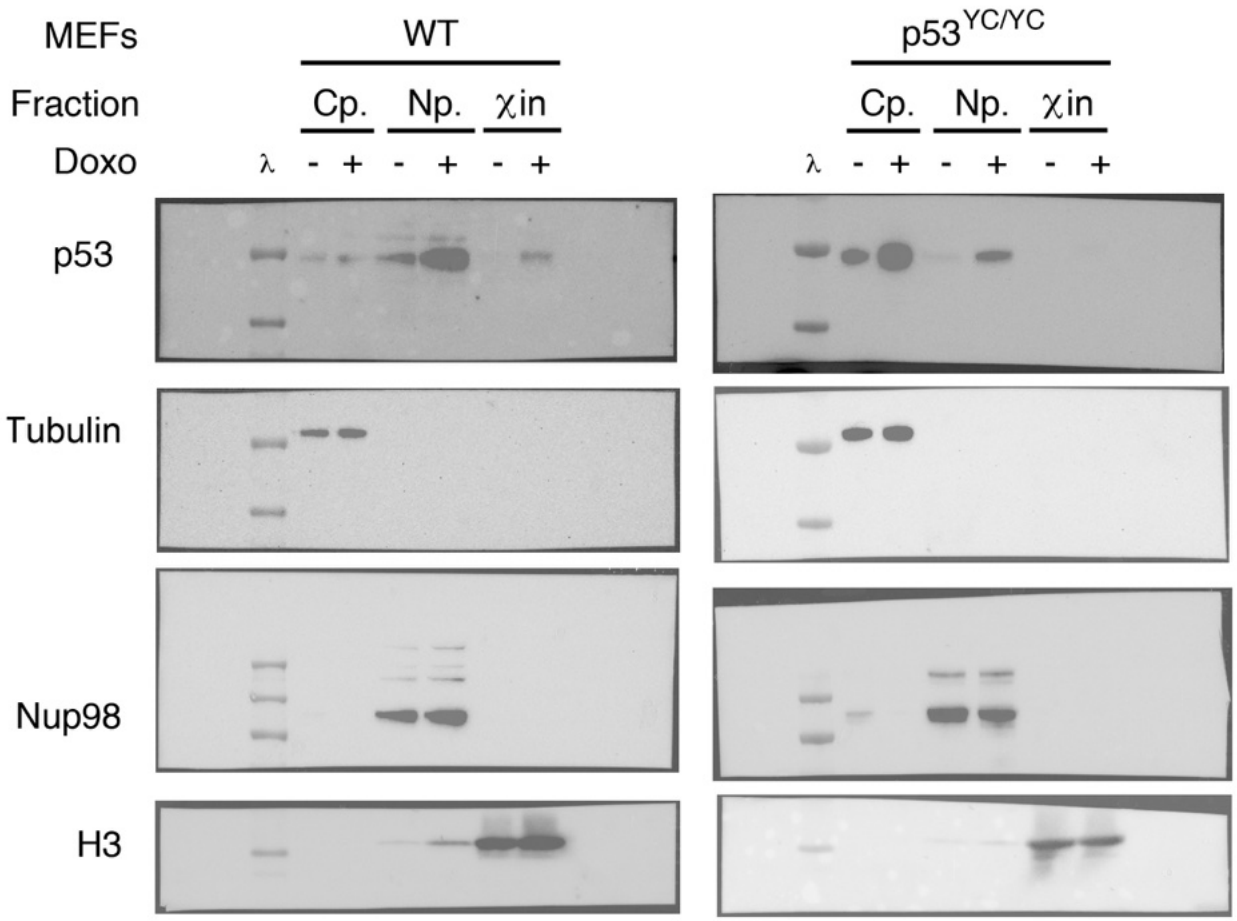

Figure S3. Uncropped images of the fractionation assays presented in Figure 2C. Chemiluminescence and colorimetric scans obtained with a ChemiDoc imaging system (Bio-Rad) were superposed to show the entire membranes, ladder lanes (λ), and chemiluminescence signals from subcellular fractions.

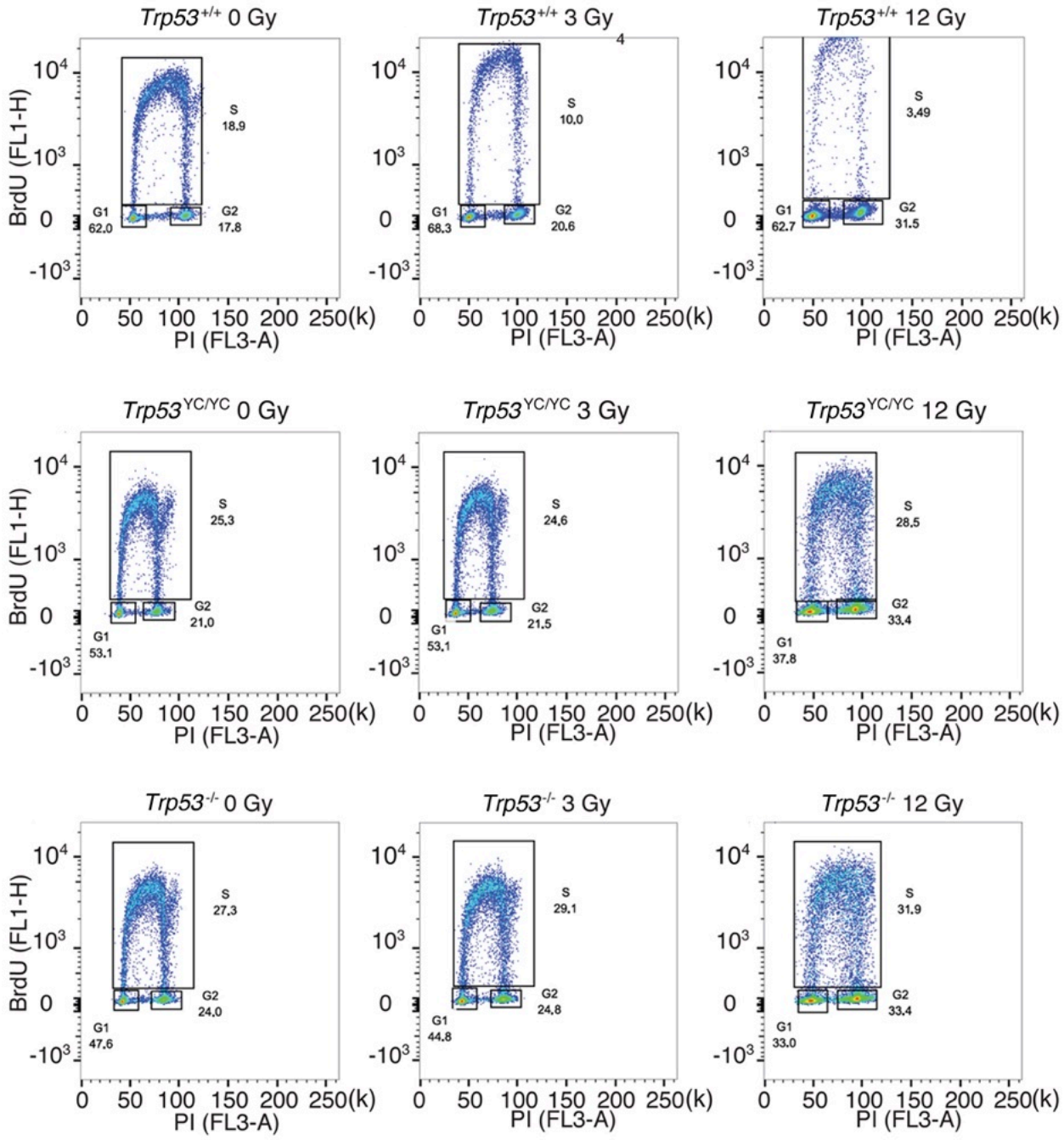

Figure S4. Cell cycle arrest responses of *Trp53*$^{+/+}$, *Trp53*$^{Y217C/Y217C}$ and *Trp53*$^{-/-}$ mouse embryonic fibroblasts.

Asynchronous MEFs were exposed to 0-12 Gy ɣ-irradiation, then after 24 hr cells were labelled with BrdU for 1 hr and analyzed by FACS. A typical experiment for cells of each genotype and condition is shown, with % cells in G1, S or G2/M mentioned in each panel.

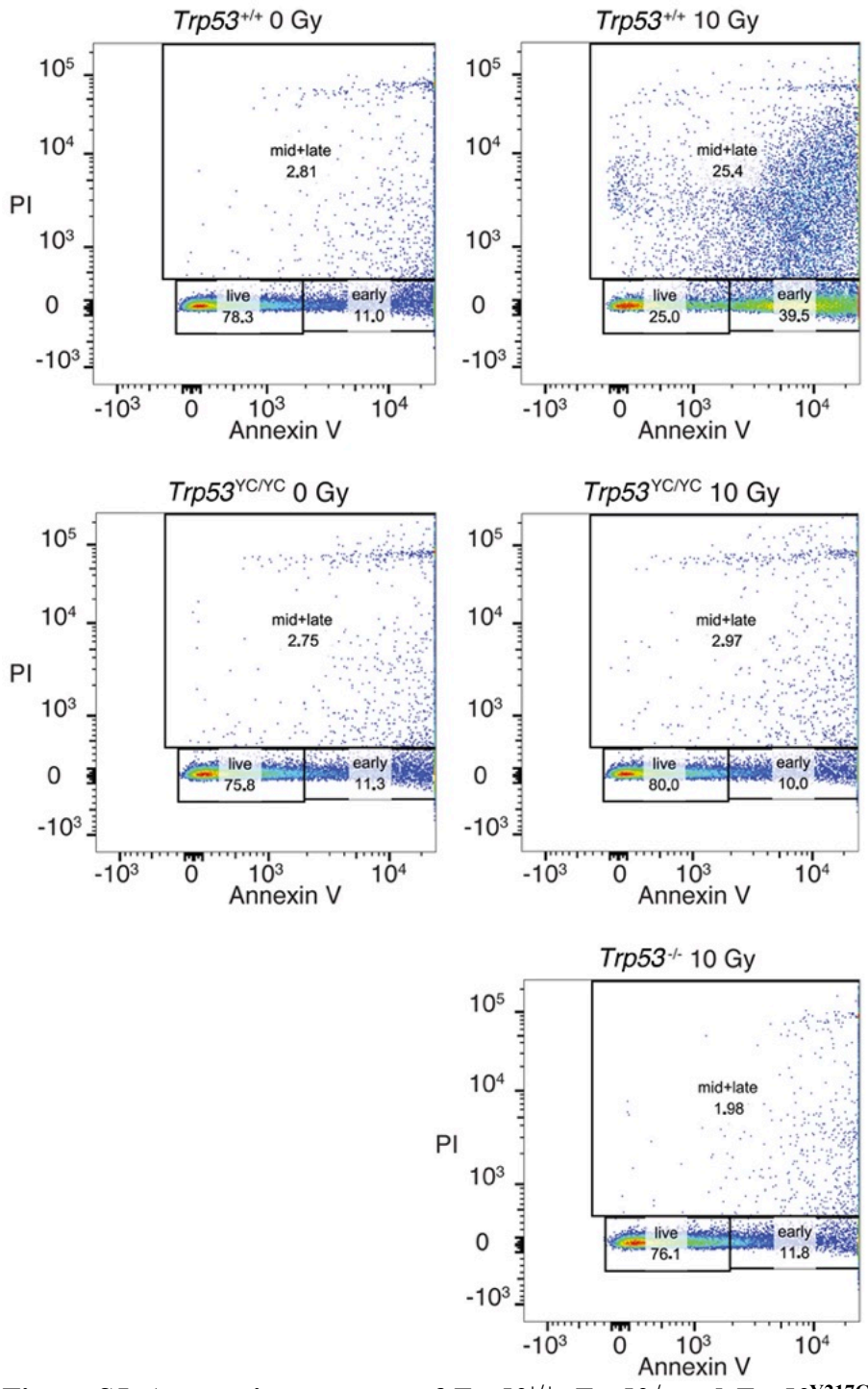

Figure S5. Apoptotic responses of *Trp53*$^{+/+}$, *Trp53*$^{-/-}$ and *Trp53*$^{Y217C/Y217C}$ thymocytes.
Mice were ɣ-irradiated (or not) and their thymocytes were recovered and analyzed by FACS after annexin V-FITC staining. A typical experiment for cells of each genotype and condition is shown. Numbers indicate % cells either alive (live), early apoptotic (early) or mid to late apoptotic (mid+late).

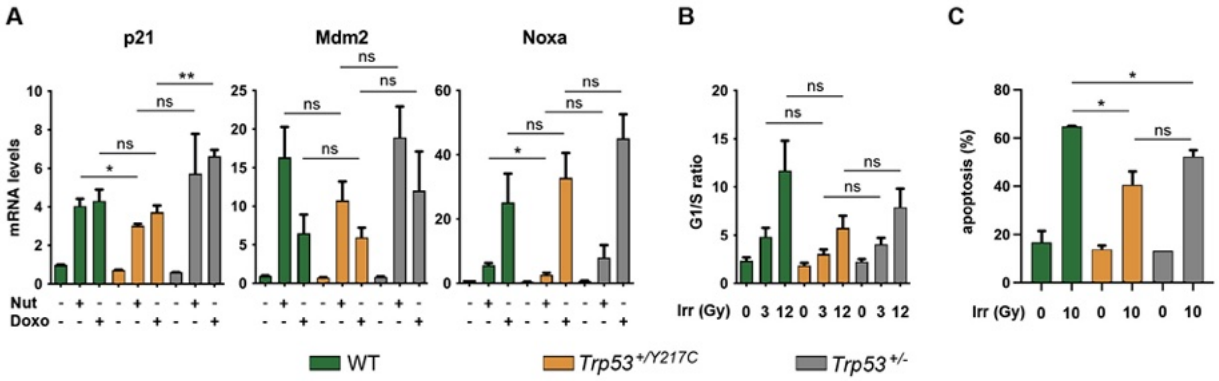

Figure S6. Comparison of stress responses in WT, *Trp53*$^{+/Y217C}$ and *Trp53*$^{+/-}$ cells.
(A) Transactivation of the classical p53 target genes *Cdkn1a/p21*, *Mdm2* and *Pmaip1*/*Noxa* in response to Nutlin or Doxorubicin. WT, *Trp53*$^{+/Y217C}$ and *Trp53*$^{+/-}$ MEFs were treated or not with 10 µM Nutlin 3a (Nut) or 1 µM Doxorubicin (Doxo) for 24 h, then mRNAs were quantified in ≥ 4 independent experiments using real-time PCR, with results normalized to control mRNAs and mean RNA amounts in unstressed WT cells assigned a value of 1. For each condition and gene, a DNE would lead to significant decrease in transactivation in *Trp53*$^{+/Y217C}$ MEFs compared to both WT and *Trp53*$^{+/-}$ MEFs, a result that was not observed. **(B)** Cell cycle arrest responses to ɣ-irradiation. Asynchronous cell populations of WT, *Trp53*$^{+/Y217C}$ and *Trp53*$^{+/-}$ MEFs were analyzed 24 hr after 0, 3 or 12 Gy ɣ-irradiation, in 3 independent experiments. The comparison of cells submitted to identical irradiation doses revealed similar arrest responses in cells of all genotypes. **(C)** Apoptotic responses to ɣ-irradiation. WT, *Trp53*$^{+/Y217C}$ and *Trp53*$^{+/-}$ MEFs age-matched mice were left untreated or submitted to 10 Gy whole-body ɣ-irradiation, then sacrificed after 4 hr and their thymocytes were stained with Annexin V-FITC and analyzed by FACS, in 2 independent experiments. The percentage of apoptotic cells was significantly higher in irradiated WT thymocytes compared to irradiated *Trp53*$^{+/Y217C}$ or *Trp53*$^{+/-}$ cells, whereas *Trp53*$^{+/Y217C}$ and *Trp53*$^{+/-}$ cells were not significantly different. **P<0.01, *P<0.05, ns: non-significant by Student's t test.

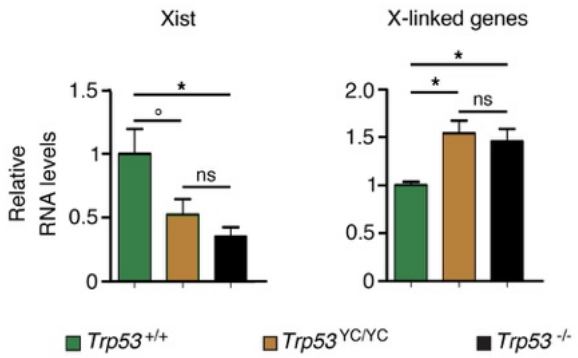

Figure S7. Evidence of aberrant chromosome X inactivation in *Trp53*$^{Y217C/Y217C}$ and *Trp53*$^{-/-}$ female embryos.

The expression of *Xist* and 3 X-linked genes (*Maob*, *Usp9x* and *Pls3*) was quantified in neurospheres from 2 *Trp53*$^{+/+}$, 5 *Trp53*$^{Y217C/Y217C}$ and 3 *Trp53*$^{-/-}$ female embryos by using real-time PCR, with results normalized to control mRNAs and mean RNA amounts in WT neurospheres assigned a value of 1. *P<0.05, °P=0.09, ns: non-significant by Student's t tests.

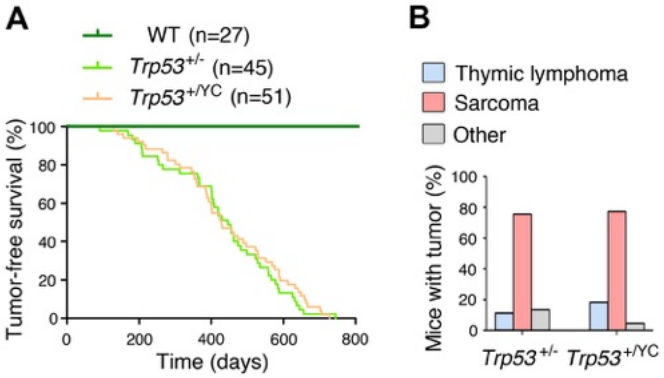

Figure S8. *Trp53*$^{+/Y217C}$ and *Trp53*$^{+/-}$ mice exhibit similar tumor onset and spectra.
No significant difference was observed between heterozygous *Trp53*$^{+/-}$ and *Trp53*$^{+/Y217C}$ mice, neither in spontaneous tumor onset and survival **(A)**, nor in tumor spectra **(B)**; n=cohort size. Mice of both sexes were included in this study.

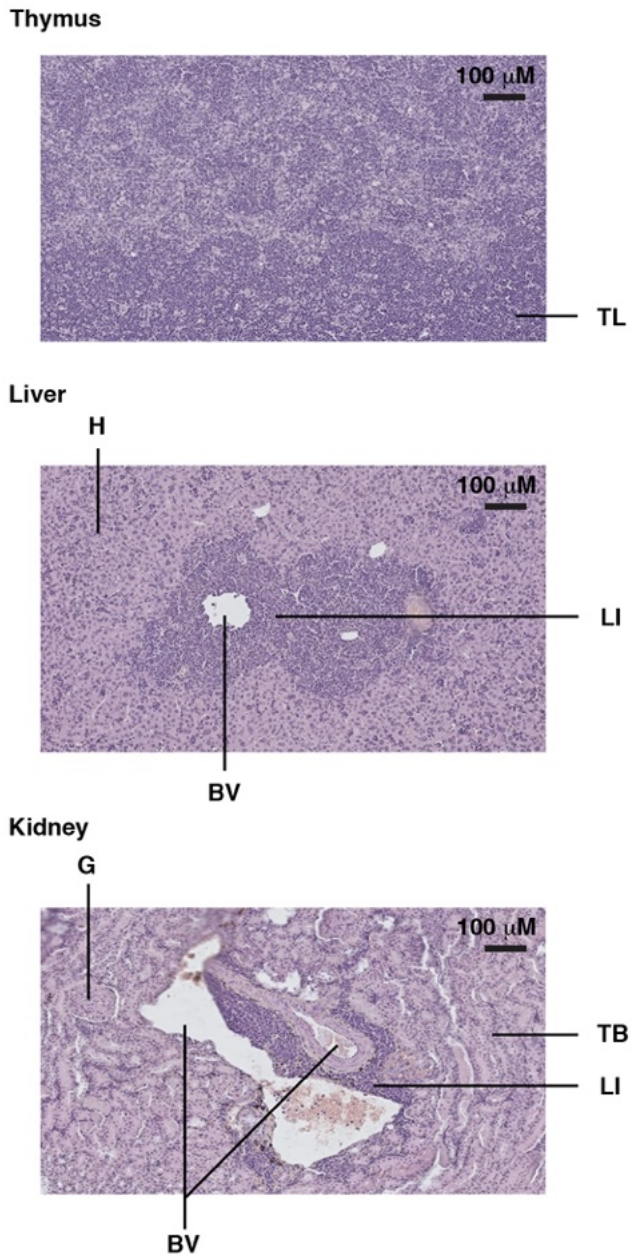

Figure S9. Example of a *Trp53*$^{Y217C/Y217C}$ mouse with a thymic lymphoma and lymphomatous infiltrates in the liver and kidney.

H&E staining of sections from the thymus (top), liver (middle) and kidney (bottom) of a *Trp53*$^{Y217C/Y217C}$ male mouse, showing tumor lymphocytes (TL) in the thymus and lymphocyte infiltrates (LI) in the liver and kidney, near blood vessels (BV). Hepatocytes (H), kidney tubules (TB) and a glomerulus (G) are also indicated.

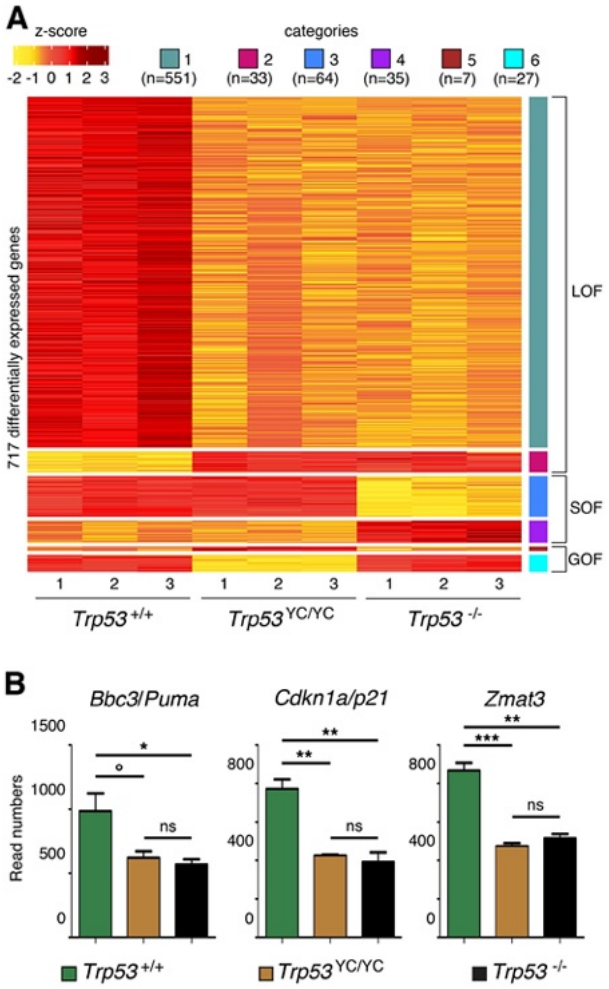

Figure S10. RNA-seq analysis from the thymi of 8 weeks-old *Trp53*$^{+/+}$, *Trp53*$^{Y217C/Y217C}$ and *Trp53*$^{-/-}$ male mice.

(A) Heat-Map plot, with 717 differentially expressed genes suggestive of a loss of function (LOF), a separation of function (SOF) or a gain of function (GOF) for the p53^{Y217C} mutant, ranked according to $\log_2$ fold change (n=number of genes). **(B)** Evidence of LOF in *Trp53*$^{Y217C/Y217C}$ cells for genes encoding Puma, p21 and Zmat3. Data from 3 mice per genotype. ***P<0.001, **P<0.01, *P<0.05, °P=0.07, ns: non-significant by Student's t tests.

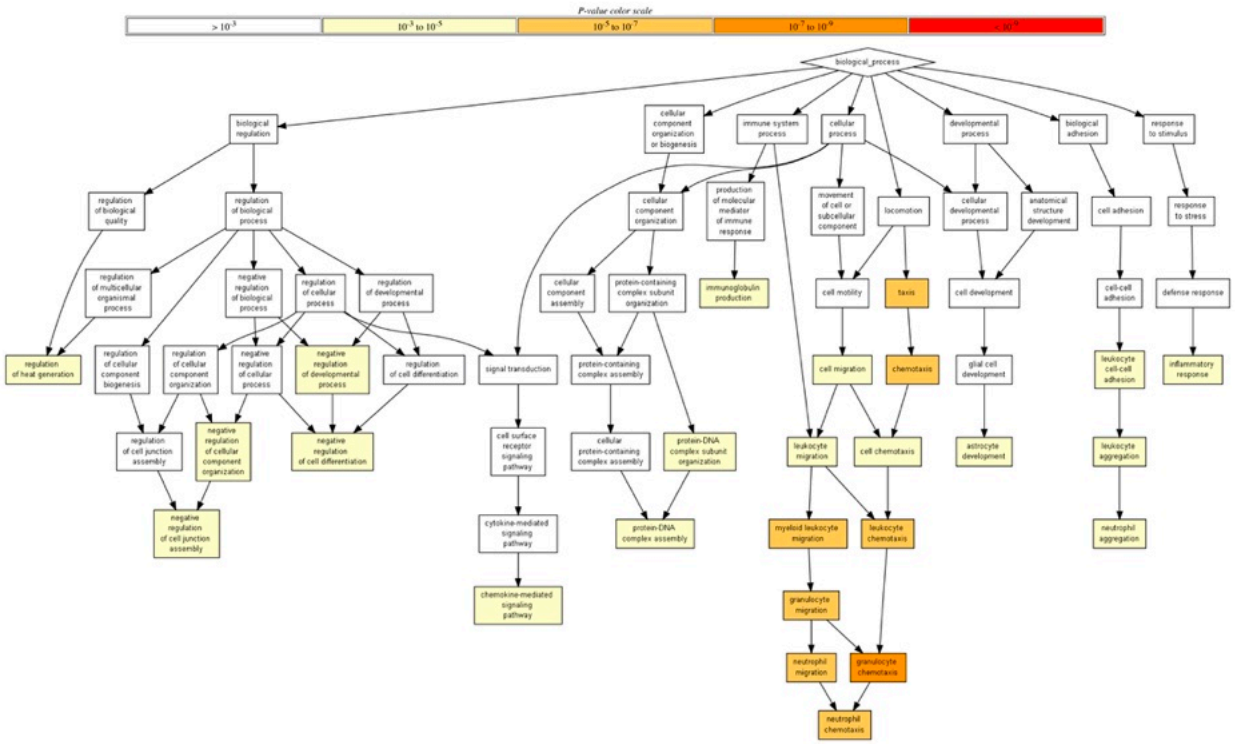

GO term	Description	P-value	FDR q-value	Enrichment (N, B, n, b)
GO:0071621	granulocyte chemotaxis	9.38E-8	1.45E-3	14.19 (19759,79,141,8)
GO:0097530	granulocyte migration	3.66E-7	2.82E-3	11.93 (19759,94,141,8)
GO:0030593	neutrophil chemotaxis	8.12E-7	4.18E-3	13.62 (19759,72,141,7)
GO:0006935	chemotaxis	1.51E-6	5.83E-3	5.66 (19759,297,141,12)
GO:0042330	taxis	1.8E-6	5.55E-3	5.57 (19759,302,141,12)
GO:0097529	myeloid leukocyte migration	2.08E-6	5.35E-3	9.50 (19759,118,141,8)
GO:1990266	neutrophil migration	2.14E-6	4.72E-3	11.82 (19759,83,141,7)
GO:0030595	leukocyte chemotaxis	3.61E-6	6.97E-3	8.83 (19759,127,141,8)
GO:0060326	cell chemotaxis	1.22E-5	2.09E-2	6.40 (19759,197,141,9)
GO:0006954	inflammatory response	4.68E-5	7.23E-2	4.02 (19759,418,141,12)
GO:0050900	leukocyte migration	8.05E-5	1.13E-1	5.75 (19759,195,141,8)
GO:0051129	negative regulation of cellular component organization	1.21E-4	1.55E-1	2.92 (19759,768,141,16)
GO:0070488	neutrophil aggregation	1.51E-4	1.79E-1	93.42 (19759,3,141,2)
GO:0070486	leukocyte aggregation	1.52E-4	1.68E-1	28.03 (19759,15,141,3)
GO:0031650	regulation of heat generation	1.86E-4	1.91E-1	26.28 (19759,16,141,3)
GO:0014002	astrocyte development	3.71E-4	3.58E-1	21.02 (19759,20,141,3)
GO:0071824	protein-DNA complex subunit organization	4.19E-4	3.81E-1	6.23 (19759,135,141,6)
GO:0045596	negative regulation of cell differentiation	4.71E-4	4.04E-1	2.69 (19759,781,141,15)
GO:0002377	immunoglobulin production	4.9E-4	3.98E-1	6.05 (19759,139,141,6)
GO:0070098	chemokine-mediated signaling pathway	5.55E-4	4.28E-1	10.58 (19759,53,141,4)
GO:1903009	negative regulation of cell junction assembly	5.67E-4	4.17E-1	18.28 (19759,23,141,3)
GO:0051093	negative regulation of developmental process	5.77E-4	4.05E-1	2.37 (19759,1064,141,18)
GO:0065004	protein-DNA complex assembly	5.97E-4	4E-1	7.38 (19759,95,141,5)
GO:0007159	leukocyte cell-cell adhesion	6.84E-4	4.4E-1	10.01 (19759,56,141,4)
GO:0016477	cell migration	9.44E-4	5.83E-1	2.51 (19759,836,141,15)

Species used: Mus musculus

The system has recognized 25139 genes out of 30795 gene terms entered by the user.
25081 genes were recognized by gene symbol and 58 genes by other gene IDs ;
239 duplicate genes were removed (keeping the highest ranking instance of each gene) leaving a total of 24900 genes.
Only 19759 of these genes are associated with a GO term.

'**P-value**' is the enrichment p-value computed according to the mHG or HG model. This p-value is not corrected for multiple testing of 15431 GO terms.

'**FDR q-value**' is the correction of the above p-value for multiple testing using the Benjamini and Hochberg (1995) method.
Namely, for the ith term (ranked according to p-value) the FDR q-value is (p-value * number of GO terms) / i.

Enrichment (N, B, n, b) is defined as follows:
N - is the total number of genes
B - is the total number of genes associated with a specific GO term
n - is the number of genes in the target set when appropriate
b - is the number of genes in the intersection
Enrichment = (b/n) / (B/N)

Figure S11. Gene ontology analysis of differentially expressed genes.
The 192 differentially expressed genes (DEGs) between *Trp53*$^{-/-}$ and *Trp53*$^{Y217C/Y217C}$ thymocytes (Fig. 5A) were analyzed with the Gene Ontology enRIchment anaLysis and visuaLizAtion tool (GOrilla). Out of 192 genes, 141 were associated with a GO term. For each GO term, enrichment was calculated by comparing with the full list of 19759 genes associated with a GO term. For example, genes with GO term #0071621 (granulocyte chemotaxis) represent 79/19759 genes associated with a GO term, but 8/141 of the identified DEGs, which represents a 14.19-fold enrichment.

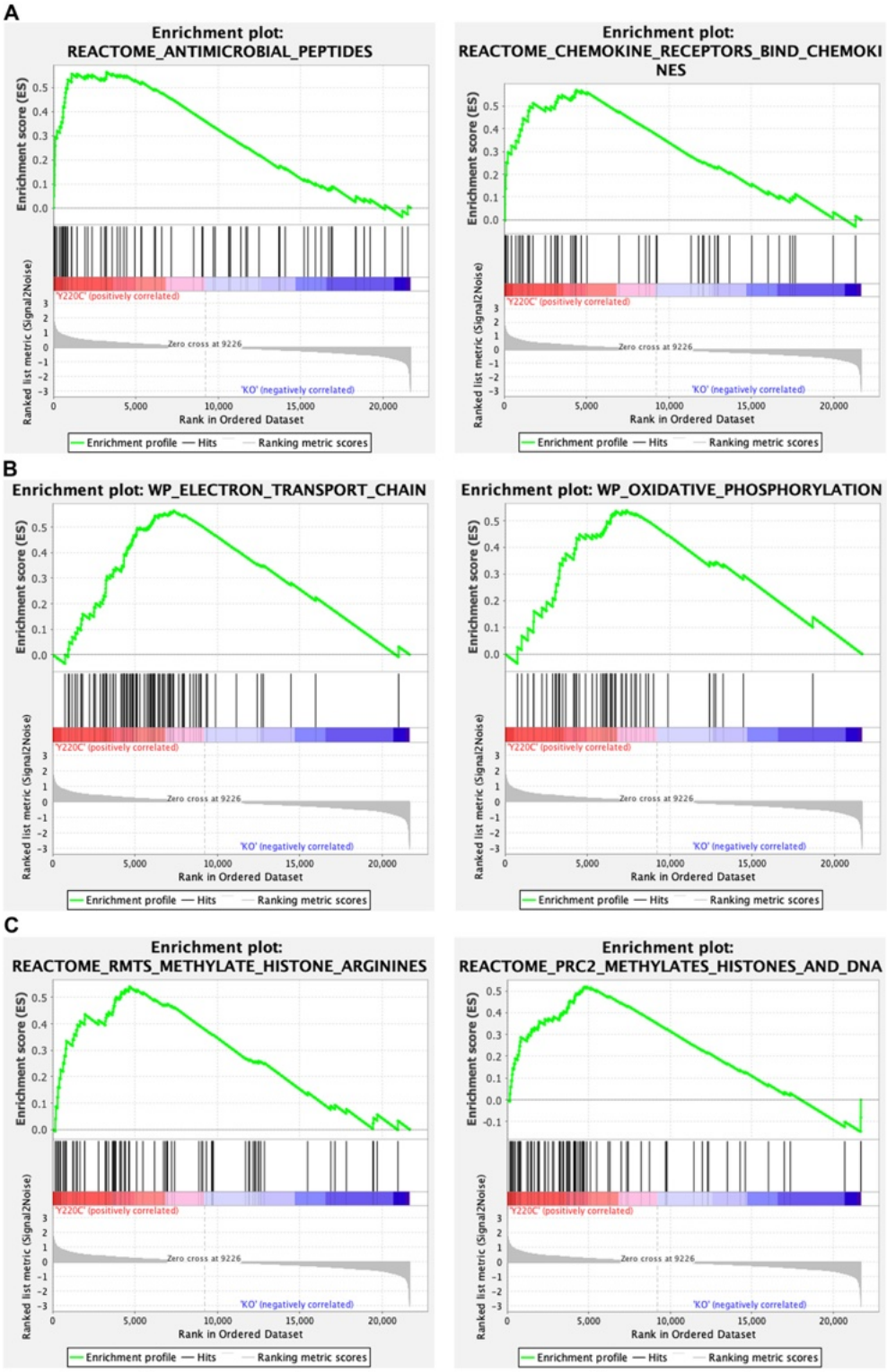

Figure S12. Gene set enrichment analysis (GSEA) of transcriptomes from *Trp53*$^{Y217C/Y217C}$ (Y220C) and *Trp53*$^{-/-}$ (KO) thymic cells: examples of GSEA enrichment plots.

Examples of GSEA enrichment plots indicating differences in immune responses **(A)**, mitochondrial function **(B)** and chromatin plasticity **(C)** are shown.

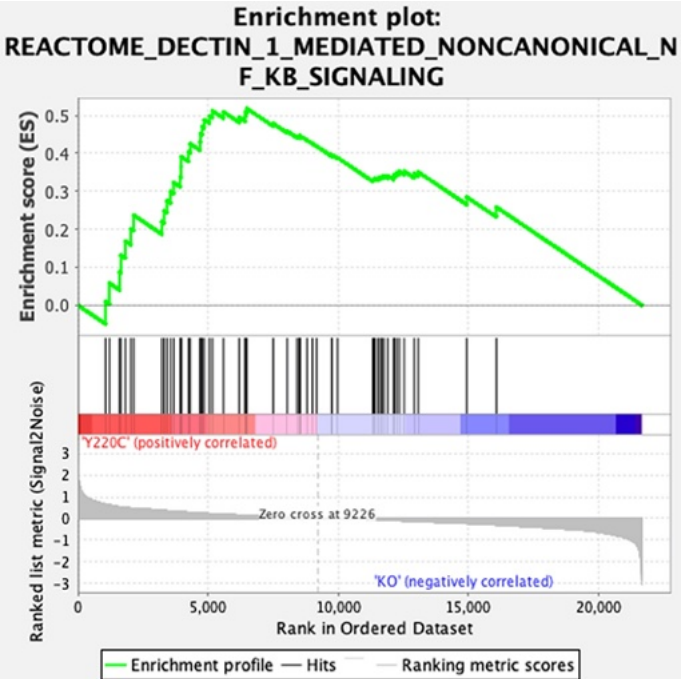

Figure S13. GSEA enrichment plot showing increased NC-NF-kB signaling in *Trp53*$^{Y217C/Y217C}$ cells.

Transcriptomes from *Trp53*$^{Y217C/Y217C}$ (Y220C) and *Trp53*$^{-/-}$ (KO) thymic cells were compared by Gene Set Enrichment Analysis.

Supplementary Tables.

at weaning

Mdm4 $^{+/-}$ ***Trp53*** $^{YC/YC}$ **x** ***Mdm4*** $^{+/-}$ ***Trp53*** $^{+/YC}$	**Nbr. females**	**Nbr. males**	**Sex ratio (f/m)**	**Total**
Mdm4 $^{+/+}$ *Trp53* $^{+/YC}$	8	11	0.73	88
Mdm4 $^{+/+}$ *Trp53* $^{YC/YC}$	0	9	0.00	
Mdm4 $^{+/-}$ *Trp53* $^{+/YC}$	15	19	0.79	
Mdm4 $^{+/-}$ *Trp53* $^{YC/YC}$	4	15	0.27	
Mdm4 $^{-/-}$ *Trp53* $^{+/YC}$	0	0	NA	
Mdm4 $^{-/-}$ *Trp53* $^{YC/YC}$	1	6	0.17	

Mdm2 $^{+/-}$ ***Trp53*** $^{YC/YC}$ **x** ***Mdm2*** $^{+/-}$ ***Trp53*** $^{+/YC}$ or ***Mdm2*** $^{-/-}$ ***Trp53*** $^{YC/YC}$ **x** ***Mdm2*** $^{+/-}$ ***Trp53*** $^{+/YC}$	**Nbr. females**	**Nbr. males**	**Sex ratio (f/m)**	**Total**
Mdm2 $^{+/+}$ *Trp53* $^{+/YC}$	3	0	NA	63
Mdm2 $^{+/+}$ *Trp53* $^{YC/YC}$	0	5	0.00	
Mdm2 $^{+/-}$ *Trp53* $^{+/YC}$	16	15	1.07	
Mdm2 $^{+/-}$ *Trp53* $^{YC/YC}$	1	11	0.09	
Mdm2 $^{-/-}$ *Trp53* $^{+/YC}$	0	0	NA	
Mdm2 $^{-/-}$ *Trp53* $^{YC/YC}$	1	11	0.09	

Table S1. Viability of Mdm2 or Mdm4 loss in a *Trp53*$^{Y217C/Y217C}$ background.
Mouse distributions from the indicated crosses were determined at weaning. As for *Trp53*$^{+/Y217C}$ intercrosses, these crosses yielded a deficit in weaned *Trp53*$^{Y217C/Y217C}$ females compared to *Trp53*$^{Y217C/Y217C}$ males (4/75 from *Trp53*$^{+/Y217C}$ intercrosses (Figure 3A); 0/9 from crosses between *Mdm4*$^{+/-}$ *Trp53*$^{+/Y217C}$ and *Mdm4*$^{+/-}$ *Trp53*$^{Y217C/Y217C}$ mice; and 0/5 from mating *Mdm2*$^{+/-}$ *Trp53*$^{+/Y217C}$ mice with *Mdm2*$^{+/-}$ *Trp53*$^{Y217C/Y217C}$ or *Mdm2*$^{-/-}$ *Trp53*$^{Y217C/Y217C}$ animals). *Trp53*$^{Y217C/Y217C}$ females over *Mdm4* or *Mdm2* deficient or haplo-insufficient backgrounds were also less frequent than their male counterparts, but the female/male ratio for *Trp53*$^{Y217C/Y217C}$ mice over a *Mdm4*$^{+/-}$ background (4/15) was significantly increased (P=0.04 when 4/75 and 4/15 ratios are compared in a Fischer's test). Whether or not the female/male ratios for *Trp53*$^{Y217C/Y217C}$ mice were significantly increased over *Mdm4*$^{-/-}$ (1/6), *Mdm2*$^{-/-}$ (1/11) or *Mdm2*$^{+/-}$ (1/11) backgrounds remained uncertain due to limited animal numbers.

F *Trp53*$^{Y217C/Y217C}$ a mated with M *Trp53*$^{+/Y217C}$	**litter 1** 1 pup born 23 days after mating was initiated, found dead (partially eaten) 24 hr later, mother is still in labor 48 hr later, another pup found dead in cage, the mother appeared in pain and was sacrificed
F *Trp53*$^{Y217C/Y217C}$ b mated with M *Trp53*$^{+/Y217C}$	**litter 1** 2 pups born 24 days after mating was initiated: 1 found dead, 1 alive (F *Trp53*$^{+/Y217C}$) **litter 2** 4 pups, all alive : 1 F *Trp53*$^{+/Y217C}$, 3 M *Trp53*$^{+/Y217C}$ **litter 3** After extended labor (24 hr) pup fragments were found in cage, the mother in pain was sacrificed with pups still inside the womb

Table S2. Evidence of dystocia in pregnant *Trp53*$^{Y217C/Y217C}$ females.
Results of the mating of two (a and b) *Trp53* $^{Y217C/Y217C}$ females (F) with a *Trp53*$^{+/Y217C}$ male (M) are shown. Both females were rapidly pregnant after encountering a male, but had to be sacrificed due to extended labor and pain during their first (female a) or third (female b) delivery.

| id | ip | geo_name | crossdomain | dnt | age | | |

Table S3. Differentially expressed genes between WT, *Trp53*$^{Y217C/Y217C}$ (YC) and *Trp53*$^{-/-}$ (KO) thymocytes from age-matched animals.

Most differentially expressed genes correspond to a loss of function (LOF) in the p53^{Y217C} mutant (categories 1 and 2, see Figure S10A), but genes corresponding to a separation of function (SOF, categories 3 and 4) or a gain of function (GOF, categories 5 and 6) were also observed.

id	gene_name	chromosome	start	end	strand	IG1_1	IG1_2	IG1_3	Y217C_1	Y217C_2	Y217C_3	Mean_KO	Mean_Y217C	Median_KO	Median_Y217C	FoldChange	logEFoldChange	FoldChangeHigh	FoldChangeLow
ENSMUSG00004ubrd10		chr8	1181583	1183570		1723.8855883	1774.867533	1816.6411633	3276960.9380	3261819.6452	2741075.0985	1689442.6395	3187670.7964	1687533.8183	2741075.0985	1.8878076964	0.8010218275	4.0300678816	0.0002136844
ENSMUSG00000Ssfb	chr17	55584025	55604204	+		7729.8835551	9016.1020964	8538.9568677	6510.0671933	6507.5421108	6587.5566932	8428.3477068	6529.369274	8538.9568677	6510.0671933	0.7746826368	-0.3660964316	0.7645396436	0.3873237176
ENSMUSG00000Aqp1	chr8	96609075	96609221	-		6692.8356461	7665.7665375	7439.9576939	5539.2603885	5479.3403088	5918.9683467	7288.4204214	5703.7483475	7665.7665375	5479.3403088	0.7756621487	-0.3685885101	0.6603235445	0.9486166876
ENSMUSG00000Ccl2	chr12	4705.7115466	4665.2041157	4776.8532667	2867.2867655	5455.2137244	3304.7767939	4667.3604256	4665.2041157	4776.8532667	3304.7767939	4887.2604256	3904.5137468	4665.2041157	4776.8532667	0.7990585232	-0.3256277491	0.6750645375	0.9463264173
ENSMUSG00000C2cd2l	chr9	44390237	44392095	-		1521.1782208	1575.9667703	1699.8138277	1109.8773944	1277.2468051	1147.8645474	1535.6869016	1175.3275771	1521.1782208	1147.8645474	0.7676222383	-0.3813315617	0.7354629018	-0.3721260816
ENSMUSG00000Ccs11	chr12	81037734	81045186	-		1564.4145432	1603.8601655	1739.1436661	1311.8888839	1295.1222223	1329.5218907	1588.7576129	1312.1989333	1603.8601655	1329.5218907	0.8255122376	-0.2750337137	0.7505148147	-0.4054253136
ENSMUSG00000Spns1	chr19	6040576	6053712	+		2154.1891381	2011.8585919	2013.4967789	2240219.1867	2261241.1851	4569592.2393	2193.0980333	2957.1298333	2013.4967789	2261241.1851	1.3484330206	0.4957969103	2.7010000000	0.6664304059
ENSMUSG00000P2rx3-ps2	chr7	75780036	75782009	-		1854.3372907	5563.1769869	5943.1658687	6449.2491018	4864.1839846	4035.0029457	5353.8910413	4349.4844021	5563.1769869	4864.1839846	1.0833893	0.1156145423	1.3215000000	0.8880000000
ENSMUSG00000Snapc4	chr2	26362765	26369053	-		9934.5856565	9391.2316776	9189.7392239	797.6086991	889.7769866	753.5777595	1855.5863230	786.7887195	1034.5865565	797.6086991	0.5369916	-0.7451319365	-0.4344146	-0.7655600058
ENSMUSG00000Ccnf	chr13	119196353	119196356	-		765.9456969	825.8025605	848.5337604	1564.1349277	1604.2024407	1556.7529	1546.5897375	1574.8266667	1564.1349277	1604.2024407	1.0182215	0.0147477527	-4.6256967674	0.0446145449
ENSMUSG00000Ubfd2	chr5	121566027	121593824	-		1089.3918613	2918.6556873	2884.1171329	2084.8345468	2318.1921455	2288.2384973	1861.8386083	2230.8465028	2318.1921455	2288.2384973	1.1982229	0.2615665	2.5232833	-0.2009165188
ENSMUSG00000Fgf13-1300mc2	chr2	25344619	25346863	-		2344.6275329	1476.8257634	1538.9636469	1844.0161133	1547.6763	1693.0665031	1453.6984	1844.9287	1538.9636469	1693.0665031	1.2688	0.3425	2.1000	0.7600
ENSMUSG00000Tox2a	chr6	49243024	49264033	-		8762.6779918	8149.2718705	8383.4465636	6391.4672232	5945.5616063	6175.7676869	8398.1834432	6220.8903555	8762.6779918	6391.4672232	0.7359663335	-0.4422883167	0.7109966864	-0.8745331911
ENSMUSG00000Ifi27	chr12	40548839	40549350	-		8103.9734	10169.0226	9355.5993	2355.7339	2355.7339	2355.7339	9355.5993	2355.7339	9355.5993	2355.7339	0.2517277	-2.1983997	0.3972000	0.0795000
ENSMUSG00000Ccl9	chr10	127531661	127621148	-		1544.3920364	1021.8794049	1050.7676968	6812.1783634	6807.2162181	8321.4037009	1205.7966867	7182.1681	1050.7676968	6812.1783634	6.0126826768	0.7781	7.2216000000	0.5551000000
ENSMUSG00000Ccl7	chr10	127531661	127621148	-		1544.3920364	1021.8794049	1050.7676968	6812.1783634	6807.2162181	8321.4037009	1205.7966867	7182.1681	1050.7676968	6812.1783634	6.0126826768	0.7781	7.2216000000	0.5551000000
ENSMUSG00000Ccl3	chr11	51204250	51236330	-		3099.8115499	1953.9364141	2335.5166966	1368.5665564	1549.2801053	1539.8183332	1129.7551814	1485.8906663	2099.8115499	1539.8183332	0.6976364844	-0.5156398832	0.4869486	0.9819000000
ENSMUSG00000Ccl4	chr11	51204250	51236330	-		3099.8115499	1953.9364141	2335.5166966	1368.5665564	1549.2801053	1539.8183332	1129.7551814	1485.8906663	2099.8115499	1539.8183332	0.6976364844	-0.5156398832	0.4869486	0.9819000000
ENSMUSG00000Ccl17	chr9	123907135	123907790	+		1325.5195928	1418.4969131	1297.2745155	3882.8882207	3882.8882207	3882.8882207	1347.1	3882.8882207	1418.4969131	3882.8882207	2.8819000000	1.5270000000	3.0000000000	0.2000000000
ENSMUSG00000Ccl8	chr9	83925145	84124240	+		464.3606666	475.3438461	537.0820788	561.7949549	587.8105410	341.7936085	488.1098623	337.1449359	475.3438461	341.7936085	0.6990802934	-0.5725264867	0.7036302628	-0.4975546776
ENSMUSG00000Ccl22	chr9	123466700	123578030	+		1294.5664561	4664.6664	7036.5624664	5664.6664	5664.6664	5664.6664	4664.6664	5664.6664	5664.6664	5664.6664	1.2142857	0.2857142857	1.7142857142	0.5714285714
ENSMUSG00000Mgat7	chr11	61488312	61494006	-		1365.6021517	3333.5603167	3266.9034495	1243.7	1026.9644945	1065.8884047	1467.1463709	1092.6366088	1332.4009	1065.8884047	0.8166666667	-0.2915	0.9166666667	-0.7333333333
ENSMUSG00000Pcbp4	chr5	20888175	20892176	+		1829.3176866	2219.6438	2197.2027	1272.1774545	1449.7678	1284.6554	2115.6	1335.7	2197.2027	1272.1774545	0.6316	-0.3425	0.9000000000	-0.5200000000
ENSMUSG00000Nhlrc	chr4	97772734	98118874	-		633.0869185	695.2513675	726.9738664	469.0464961	468.7479324	521.4384606	718.4119441	486.4164444	695.2513675	468.9464961	0.6766869283	-0.5636051237	0.6969196116	-0.5153573146
ENSMUSG00000Ccl5	chr5	91948275	91958756	-		3585.3535456	3382.4469236	2763.4149	3987.3854924	3456.7673	3521.7365	3243.7	3655.7	3382.4469236	3521.7365	1.0863000000	0.1200000000	1.5000000000	0.6700000000
ENSMUSG00000Ccl2	chr5	91948275	91958756	-		3585.3535456	3382.4469236	2763.4149	3987.3854924	3456.7673	3521.7365	3243.7	3655.7	3382.4469236	3521.7365	1.0863000000	0.1200000000	1.5000000000	0.6700000000
ENSMUSG00000Ccl4spa3	chr17	25343659	25356364	-		1314.8322358	1592.3121339	1385.8636281	6125.0660217	6164.7938	6164.7938	1430.9669139	6485.6921	1385.8636281	6164.7938	4.3000000000	1.6000000000	6.0000000000	0.2000000000
ENSMUSG00000Ccl5gs	chr5	73957920	73974804	-		8885.8837579	4484.8136033	5640.4185397	8636.9903	8636.9903	8636.9903	5336.9051	8636.9903	8636.9903	8636.9903	1.6179999	0.6250733571	2.5189999999	0.3810000000
ENSMUSG00000Ccl5mirv	chr5	73957920	73974804	-		8885.8837579	4484.8136033	5640.4185397	8636.9903	8636.9903	8636.9903	5336.9051	8636.9903	8636.9903	8636.9903	1.6179999	0.6250733571	2.5189999999	0.3810000000
ENSMUSG00000Ccl4rw	chr5	73957919	73974468	+		1531.6816373	1673.3609171	1941.2729553	1017.6784273	1171.2396669	1166.5296939	1756.7109119	1118.4791419	1673.3609171	1166.5296939	0.6638324008	-0.6352429969	0.6851595029	-0.5317342021
ENSMUSG00000Smarbq	chr2	84889091	85003207	+		2172.3524627	3111.4623535	3068.9486208	4868.7728	4868.7728	4868.7728	3109.7	4868.7728	3111.4623535	4868.7728	1.5655000000	0.6500000000	2.3000000000	0.4000000000
ENSMUSG00000Ccl1	chr9	123907135	123907790	+		1325.5195928	1418.4969131	1297.2745155	3882.8882207	3882.8882207	3882.8882207	1347.1	3882.8882207	1418.4969131	3882.8882207	2.8819000000	1.5270000000	3.0000000000	0.2000000000
ENSMUSG00000Ccl11	chr9	123466700	123578030	+		1294.5664561	4664.6664	7036.5624664	5664.6664	5664.6664	5664.6664	4664.6664	5664.6664	5664.6664	5664.6664	1.2142857	0.2857142857	1.7142857142	0.5714285714
ENSMUSG00000Ccl24	chr9	123466700	123578030	+		1294.5664561	4664.6664	7036.5624664	5664.6664	5664.6664	5664.6664	4664.6664	5664.6664	5664.6664	5664.6664	1.2142857	0.2857142857	1.7142857142	0.5714285714
ENSMUSG00000Ccl26	chr9	123466700	123578030	+		1294.5664561	4664.6664	7036.5624664	5664.6664	5664.6664	5664.6664	4664.6664	5664.6664	5664.6664	5664.6664	1.2142857	0.2857142857	1.7142857142	0.5714285714
ENSMUSG00000Ccl6	chr10	127531661	127621148	-		1544.3920364	1021.8794049	1050.7676968	6812.1783634	6807.2162181	8321.4037009	1205.7966867	7182.1681	1050.7676968	6812.1783634	6.0126826768	0.7781	7.2216000000	0.5551000000
ENSMUSG00000Ccl9ilp	chr11	103945506	103955620	+		387.7992794	239.1364551	251.3974846	116.9824719	108.9561145	108.1545436	492.9333587	113.2285526	239.1364551	108.1545436	0.4857455953	-1.1528355	0.4993825547	-1.9348000000
ENSMUSG00000Ccl7-ps1	chr10	127531661	127621148	-		1544.3920364	1021.8794049	1050.7676968	6812.1783634	6807.2162181	8321.4037009	1205.7966867	7182.1681	1050.7676968	6812.1783634	6.0126826768	0.7781	7.2216000000	0.5551000000
ENSMUSG00000Ccl4rt	chr10	89985243	89987648	+		107.9696828	95.6471236	94.7314946	68.7396782	68.9726598	51.3272774	145.9076193	63.0095313	104.7134946	68.7396782	0.4296384	-1.2180506	0.7635290	-1.3863206
ENSMUSG00000Ccl4spa2	chr17	25343356	25346659	-		3866.7015176	3896.0529313	3339.7227618	7556654.117	8008269.145	7601576.980	3700.1514	7722	3896.0529313	7556654.117	2050.0000000	11.0000000000	2050.0000000	0.0000000000
ENSMUSG00000Ccl4spa-ps1	chr17	25343356	25346659	-		3866.7015176	3896.0529313	3339.7227618	7556654.117	8008269.145	7601576.980	3700.1514	7722	3896.0529313	7556654.117	2050.0000000	11.0000000000	2050.0000000	0.0000000000
ENSMUSG00000Ccl4spa-ps2	chr17	25343356	25346659	-		3866.7015176	3896.0529313	3339.7227618	7556654.117	8008269.145	7601576.980	3700.1514	7722	3896.0529313	7556654.117	2050.0000000	11.0000000000	2050.0000000	0.0000000000
ENSMUSG00000Ccl4spa-ps3	chr17	25343356	25346659	-		3866.7015176	3896.0529313	3339.7227618	7556654.117	8008269.145	7601576.980	3700.1514	7722	3896.0529313	7556654.117	2050.0000000	11.0000000000	2050.0000000	0.0000000000
ENSMUSG00000Ccl4rt-ps1	chr10	89985243	89987648	+		107.9696828	95.6471236	94.7314946	68.7396782	68.9726598	51.3272774	145.9076193	63.0095313	104.7134946	68.7396782	0.4296384	-1.2180506	0.7635290	-1.3863206
ENSMUSG00000Ccl4rt-ps2	chr10	89985243	89987648	+		107.9696828	95.6471236	94.7314946	68.7396782	68.9726598	51.3272774	145.9076193	63.0095313	104.7134946	68.7396782	0.4296384	-1.2180506	0.7635290	-1.3863206
ENSMUSG00000Ccl4rt-ps3	chr10	89985243	89987648	+		107.9696828	95.6471236	94.7314946	68.7396782	68.9726598	51.3272774	145.9076193	63.0095313	104.7134946	68.7396782	0.4296384	-1.2180506	0.7635290	-1.3863206
ENSMUSG00000Ccl4rt-ps4	chr10	89985243	89987648	+		107.9696828	95.6471236	94.7314946	68.7396782	68.9726598	51.3272774	145.9076193	63.0095313	104.7134946	68.7396782	0.4296384	-1.2180506	0.7635290	-1.3863206
ENSMUSG00000Ccl4rt-ps5	chr10	89985243	89987648	+		107.9696828	95.6471236	94.7314946	68.7396782	68.9726598	51.3272774	145.9076193	63.0095313	104.7134946	68.7396782	0.4296384	-1.2180506	0.7635290	-1.3863206
ENSMUSG00000Ccl4rt-ps6	chr10	89985243	89987648	+		107.9696828	95.6471236	94.7314946	68.7396782	68.9726598	51.3272774	145.9076193	63.0095313	104.7134946	68.7396782	0.4296384	-1.2180506	0.7635290	-1.3863206
ENSMUSG00000Ccl4rt-ps7	chr10	89985243	89987648	+		107.9696828	95.6471236	94.7314946	68.7396782	68.9726598	51.3272774	145.9076193	63.0095313	104.7134946	68.7396782	0.4296384	-1.2180506	0.7635290	-1.3863206
ENSMUSG00000Ccl4rt-ps8	chr10	89985243	89987648	+		107.9696828	95.6471236	94.7314946	68.7396782	68.9726598	51.3272774	145.9076193	63.0095313	104.7134946	68.7396782	0.4296384	-1.2180506	0.7635290	-1.3863206
ENSMUSG00000Ccl4rt-ps9	chr10	89985243	89987648	+		107.9696828	95.6471236	94.7314946	68.7396782	68.9726598	51.3272774	145.9076193	63.0095313	104.7134946	68.7396782	0.4296384	-1.2180506	0.7635290	-1.3863206
ENSMUSG00000Ccl4rt-ps10	chr10	89985243	89987648	+		107.9696828	95.6471236	94.7314946	68.7396782	68.9726598	51.3272774	145.9076193	63.0095313	104.7134946	68.7396782	0.4296384	-1.2180506	0.7635290	-1.3863206
ENSMUSG00000Ccl4rt-ps11	chr10	89985243	89987648	+		107.9696828	95.6471236	94.7314946	68.7396782	68.9726598	51.3272774	145.9076193	63.0095313	104.7134946	68.7396782	0.4296384	-1.2180506	0.7635290	-1.3863206
ENSMUSG00000Ccl4rt-ps12	chr10	89985243	89987648	+		107.9696828	95.6471236	94.7314946	68.7396782	68.9726598	51.3272774	145.9076193	63.0095313	104.7134946	68.7396782	0.4296384	-1.2180506	0.7635290	-1.3863206
ENSMUSG00000Ccl4rt-ps13	chr10	89985243	89987648	+		107.9696828	95.6471236	94.7314946	68.7396782	68.9726598	51.3272774	145.9076193	63.0095313	104.7134946	68.7396782	0.4296384	-1.2180506	0.7635290	-1.3863206
ENSMUSG00000Ccl4rt-ps14	chr10	89985243	89987648	+		107.9696828	95.6471236	94.7314946	68.7396782	68.9726598	51.3272774	145.9076193	63.0095313	104.7134946	68.7396782	0.4296384	-1.2180506	0.7635290	-1.3863206
ENSMUSG00000Ccl4rt-ps15	chr10	89985243	89987648	+		107.9696828	95.6471236	94.7314946	68.7396782	68.9726598	51.3272774	145.9076193	63.0095313	104.7134946	68.7396782	0.4296384	-1.2180506	0.7635290	-1.3863206
ENSMUSG00000Ccl4rt-ps16	chr10	89985243	89987648	+		107.9696828	95.6471236	94.7314946	68.7396782	68.9726598	51.3272774	145.9076193	63.0095313	104.7134946	68.7396782	0.4296384	-1.2180506	0.7635290	-1.3863206
ENSMUSG00000Ccl4rt-ps17	chr10	89985243	89987648	+		107.9696828	95.6471236	94.7314946	68.7396782	68.9726598	51.3272774	145.9076193	63.0095313	104.7134946	68.7396782	0.4296384	-1.2180506	0.7635290	-1.3863206
ENSMUSG00000Ccl4rt-ps18	chr10	89985243	89987648	+		107.9696828	95.6471236	94.7314946	68.7396782	68.9726598	51.3272774	145.9076193	63.0095313	104.7134946	68.7396782	0.4296384	-1.2180506	0.7635290	-1.3863206
ENSMUSG00000Ccl4rt-ps19	chr10	89985243	89987648	+		107.9696828	95.6471236	94.7314946	68.7396782	68.9726598	51.3272774	145.9076193	63.0095313	104.7134946	68.7396782	0.4296384	-1.2180506	0.7635290	-1.3863206
ENSMUSG00000Ccl4rt-ps20	chr10	89985243	89987648	+		107.9696828	95.6471236	94.7314946	68.7396782	68.9726598	51.3272774	145.9076193	63.0095313	104.7134946	68.7396782	0.4296384	-1.2180506	0.7635290	-1.3863206
ENSMUSG00000Ccl4rt-ps21	chr10	89985243	89987648	+		107.9696828	95.6471236	94.7314946	68.7396782	68.9726598	51.3272774	145.9076193	63.0095313	104.7134946	68.7396782	0.4296384	-1.2180506	0.7635290	-1.3863206
ENSMUSG00000Ccl4rt-ps22	chr10	89985243	89987648	+		107.9696828	95.6471236	94.7314946	68.7396782	68.9726598	51.3272774	145.9076193	63.0095313	104.7134946	68.7396782	0.4296384	-1.2180506	0.7635290	-1.3863206
ENSMUSG00000Ccl4rt-ps23	chr10	89985243	89987648	+		107.9696828	95.6471236	94.7314946	68.7396782	68.9726598	51.3272774	145.9076193	63.0095313	104.7134946	68.7396782	0.4296384	-1.2180506	0.7635290	-1.3863206
ENSMUSG00000Ccl4rt-ps24	chr10	89985243	89987648	+		107.9696828	95.6471236	94.7314946	68.7396782	68.9726598	51.3272774	145.9076193	63.0095313	104.7134946	68.7396782	0.4296384	-1.2180506	0.7635290	-1.3863206
ENSMUSG00000Ccl4rt-ps25	chr10	89985243	89987648	+		107.9696828	95.6471236	94.7314946	68.7396782	68.9726598	51.3272774	145.9076193	63.0095313	104.7134946	68.7396782	0.4296384	-1.2180506	0.7635290	-1.3863206
ENSMUSG00000Ccl4rt-ps26	chr10	89985243	89987648	+		107.9696828	95.6471236	94.7314946	68.7396782	68.9726598	51.3272774	145.9076193	63.0095313	104.7134946	68.7396782	0.4296384	-1.2180506	0.7635290	-1.3863206
ENSMUSG00000Ccl4rt-ps27	chr10	89985243	89987648	+		107.9696828	95.6471236	94.7314946	68.7396782	68.9726598	51.3272774	145.9076193	63.0095313	104.7134946	68.7396782	0.4296384	-1.2180506	0.7635290	-1.3863206
ENSMUSG00000Ccl4rt-ps28	chr10	89985243	89987648	+		107.9696828	95.6471236	94.7314946	68.7396782	68.9726598	51.3272774	145.9076193	63.0095313	104.7134946	68.7396782	0.4296384	-1.2180506	0.7635290	-1.3863206
ENSMUSG00000Ccl4rt-ps29	chr10	89985243	89987648	+		107.9696828	95.6471236	94.7314946	68.7396782	68.9726598	51.3272774	145.9076193	63.0095313	104.7134946	68.7396782	0.4296384	-1.2180506	0.7635290	-1.3863206
ENSMUSG00000Ccl4rt-ps30	chr10	89985243	89987648	+		107.9696828	95.6471236	94.7314946	68.7396782	68.9726598	51.3272774	145.9076193	63.0095313	104.7134946	68.7396782	0.4296384	-1.2180506	0.7635290	-1.3863206
ENSMUSG00000Ccl4rt-ps31	chr10	89985243	89987648	+		107.9696828	95.6471236	94.7314946	68.7396782	68.9726598	51.3272774	145.9076193	63.0095313	104.7134946	68.7396782	0.4296384	-1.2180506	0.7635290	-1.3863206
ENSMUSG00000Ccl4rt-ps32	chr10	89985243	89987648	+		107.9696828	95.6471236	94.7314946	68.7396782	68.9726598	51.3272774	145.9076193	63.0095313	104.7134946	68.7396782	0.4296384	-1.2180506	0.7635290	-1.3863206
ENSMUSG00000Ccl4rt-ps33	chr10	89985243	89987648	+		107.9696828	95.6471236	94.7314946	68.7396782	68.9726598	51.3272774	145.9076193	63.0095313	104.7134946	68.7396782	0.4296384	-1.2180506	0.7635290	-1.3863206
ENSMUSG00000Ccl4rt-ps34	chr10	89985243	89987648	+		107.9696828	95.6471236	94.7314946	68.7396782	68.9726598	51.3272774	145.9076193	63.0095313	104.7134946	68.7396782	0.4296384	-1.2180506	0.7635290	-1.3863206
ENSMUSG00000Ccl4rt-ps35	chr10	89985243	89987648	+		107.9696828	95.6471236	94.7314946	68.7396782	68.9726598	51.3272774	145.9076193	63.0095313	104.7134946	68.7396782	0.4296384	-1.2180506	0.7635290	-1.3863206
ENSMUSG00000Ccl4rt-ps36	chr10	89985243	89987648	+		107.9696828	95.6471236	94.7314946	68.7396782	68.9726598	51.3272774	145.9076193	63.0095313	104.7134946	68.7396782	0.4296384	-1.2180506	0.7635290	-1.3863206
ENSMUSG00000Ccl4rt-ps37	chr10	89985243	89987648	+		107.9696828	95.6471236	94.7314946	68.7396782	68.9726598	51.3272774	145.9076193	63.0095313	104.7134946	68.7396782	0.4296384	-1.2180506	0.7635290	-1.3863206
ENSMUSG00000Ccl4rt-ps38	chr10	89985243	89987648	+		107.9696828	95.6471236	94.7314946	68.7396782	68.9726598	51.3272774	145.9076193	63.0095313	104.7134946	68.7396782	0.4296384	-1.2180506	0.7635290	-1.3863206
ENSMUSG00000Ccl4rt-ps39	chr10	89985243	89987648	+		107.9696828	95.6471236	94.7314946	68.7396782	68.9726598	51.3272774	145.9076193	63.0095313	104.7134946	68.7396782	0.4296384	-1.2180506	0.7635290	-1.3863206
ENSMUSG00000Ccl4rt-ps40	chr10	89985243	89987648	+		107.9696828	95.6471236	94.7314946	68.7396782	68.9726598	51.3272774	145.9076193	63.0095313	104.7134946	68.7396782	0.4296384	-1.2180506	0.7635290	-1.3863206
ENSMUSG00000Ccl4rt-ps41	chr10	89985243	89987648	+		107.9696828	95.6471236	94.7314946	68.7396782	68.9726598	51.3272774	145.9076193	63.0095313	104.7134946	68.7396782	0.4296384	-1.2180506	0.7635290	-1.3863206
ENSMUSG00000Ccl4rt-ps42	chr10	89985243	89987648	+		107.9696828	95.6471236	94.7314946	68.7396782	68.9726598	51.3272774	145.9076193	63.0095313	104.7134946	68.7396782	0.4296384	-1.2180506	0.7635290	-1.3863206
ENSMUSG00000Ccl4rt-ps43	chr10	89985243	89987648	+		107.9696828	95.6471236	94.7314946	68.7396782	68.9726598	51.3272774	145.9076193	63.0095313	104.7134946	68.7396782	0.4296384	-1.2180506	0.7635290	-1.3863206
ENSMUSG00000Ccl4rt-ps44	chr10	89985243	89987648	+		107.9696828	95.6471236	94.7314946	68.7396782	68.9726598	51.3272774	145.9076193	63.0095313	104.7134946	68.7396782	0.4296384	-1.2180506	0.7635290	-1.3863206
ENSMUSG00000Ccl4rt-ps45	chr10	89985243	89987648	+		107.9696828	95.6471236	94.7314946	68.7396782	68.9726598	51.3272774	145.9076193	63.0095313	104.7134946	68.7396782	0.4296384	-1.2180506	0.7635290	-1.3863206
ENSMUSG00000Ccl4rt-ps46	chr10	89985243	89987648	+		107.9696828	95.6471236	94.7314946	68.7396782	68.9726598	51.3272774	145.9076193	63.0095313	104.7134946	68.7396782	0.4296384	-1.2180506	0.7635290	-1.3863206
ENSMUSG00000Ccl4rt-ps47	chr10	89985243	89987648	+		107.9696828	95.6471236	94.7314946	68.7396782	68.9726598	51.3272774	145.9076193	63.0095313	104.7134946	68.7396782	0.4296384	-1.2180506	0.7635290	-1.3863206
ENSMUSG00000Ccl4rt-ps48	chr10	89985243	89987648	+		107.9696828	95.6471236	94.7314946	68.7396782	68.9726598	51.3272774	145.9076193	63.0095313	104.7134946	68.7396782	0.4296384	-1.2180506	0.7635290	-1.3863206
ENSMUSG00000Ccl4rt-ps49	chr10	89985243	89987648	+		107.9696828	95.6471236	94.7314946	68.7396782	68.9726598	51.3272774	145.9076193	63.0095313	104.7134946	68.7396782	0.4296384	-1.2180506	0.7635290	-1.3863206
ENSMUSG00000Ccl4rt-ps50	chr10	89985243	89987648	+		107.9696828	95.6471236	94.7314946	68.7396782	68.9726598	51.3272774	145.9076193	63.0095313	104.7134946	68.7396782	0.4296384	-1.2180506	0.7635290	-1.3863206
ENSMUSG00000Ccl4rt-ps51	chr10	89985243	89987648	+		107.9696828	95.6471236	94.7314946	68.7396782	68.9726598	51.3272774	145.9076193	63.0095313	104.7134946	68.7396782	0.4296384	-1.2180506	0.7635290	-1.3863206
ENSMUSG00000Ccl4rt-ps52	chr10	89985243	89987648	+		107.9696828	95.6471236	94.7314946	68.7396782	68.9726598	51.3272774	145.9076193	63.0095313	104.7134946	68.7396782	0.4296384	-1.2180506	0.7635290	-1.3863206
ENSMUSG00000Ccl4rt-ps53	chr10	89985243	89987648	+		107.9696828	95.6471236	94.7314946	68.7396782	68.9726598	51.3272774	145.9076193	63.0095313	104.7134946	68.7396782	0.4296384	-1.2180506	0.7635290	-1.3863206
ENSMUSG00000Ccl4rt-ps54	chr10	89985243	89987648	+		107.9696828	95.6471236	94.7314946	68.7396782	68.9726598	51.3272774	145.9076193	63.0095313	104.7134946	68.7396782	0.4296384	-1.2180506	0.7635290	-1.3863206
ENSMUSG00000Ccl4rt-ps55	chr10	89985243	89987648	+		107.9696828	95.6471236	94.7314946	68.7396782	68.9726598	51.3272774	145.9076193	63.0095313	104.7134946	68.7396782	0.4296384	-1.2180506	0.7635290	-1.3863206
ENSMUSG00000Ccl4rt-ps56	chr10	89985243	89987648	+		107.9696828	95.6471236	94.7314946	68.7396782	68.9726598	51.3272774	145.9076193	63.0095313	104.7134946	68.7396782	0.4296384	-1.2180506	0.7635290	-1.3863206
ENSMUSG00000Ccl4rt-ps57	chr10	89985243	89987648	+		107.9696828	95.6471236	94.7314946	68.7396782	68.9726598	51.3272774	145.9076193	63.0095313	104.7134946	68.7396782	0.4296384	-1.2180506	0.7635290	-1.3863206
ENSMUSG00000Ccl4rt-ps58	chr10	89985243	89987648	+		107.9696828

GO term	Description	*Ccl17*	*Ccl9*	*Ccr3*	*Cxcl10*	*S100a8*	*S100a9*
GO:0071621	granulocyte chemotaxis	x	x	x	x	x	x
GO:0097530	granulocyte migration	x	x	x	x	x	x
GO:0030593	neutrophil chemotaxis	x	x		x	x	x
GO:0006935	chemotaxis	x	x	x	x	x	x
GO:0042330	taxis	x	x	x	x	x	x
GO:0097529	myeloid leukocyte migration	x	x	x	x	x	x
GO:1990266	neutrophil migration	x	x		x	x	x
GO:0030595	leukocyte chemotaxis	x	x	x	x	x	x
GO:0060326	cell chemotaxis	x	x	x	x	x	x
GO:0006954	inflammatory response	x	x	x	x	x	x
GO:0050900	leukocyte migration	x	x	x	x	x	x
GO:0070488	neutrophil aggregation					x	x
GO:0070486	leukocyte aggregation					x	x
GO:0070098	chemokine-mediated signaling pathway	x	x		x		
GO:0007159	leukocyte cell-cell adhesion					x	x
GO:0016477	cell migration	x	x	x	x	x	x

Table S5. *Ccl17*, *Ccl9*, *Ccr3*, *Cxcl10*, *S100a8* and *S100a9* are associated with GO terms of white blood cell migration/chemotaxis and inflammation.

at weaning

F *Trp53* $^{+/YC}$ x M *Trp53* $^{YC/YC}$	Nbr. Females (SIU+)	Nbr. Males (SIU+)	Sex ratio (f/m)	Total
Trp53 $^{+/YC}$	26	17	1.53	59
Trp53 $^{YC/YC}$	3	13	0.23	

Table S6. Distribution of weaned pups after mating *Trp53*$^{+/Y217C}$ females with *Trp53*$^{Y217C/Y217C}$ males and oral gavage of pregnant females with supformin.

Due to the gavage of pregnant mothers, all the pups born in this experiment were exposed to supformin *in utero* (SIU+).

Trp53 $^{-/-}$ (LOF)	*Trp53* $^{Y217C/Y217C}$ (LOF+GOF)
spontaneous tumors (mostly thymic lymphomas), death in ≤ 1 year. ++ (M & F)	spontaneous tumors (mostly thymic lymphomas) with metastases, death in ≤ 7 months. +++ (only M were evaluated due to scarcity of F) inflammation in thymic cells
perinatal lethality + (F only : Xi aberrations)	perinatal lethality increased ++++ (F only : Xi aberrations and inflammation) F partial rescue by supformin
no dystocia (pregnant F)	dystocia + (pregnant F)

Table S7. Effects of the *Trp53*^{Y217C} mutation: a summary.
The comparison between *Trp53*$^{-/-}$ and *Trp53*$^{Y217C/Y217C}$ mice is presented. The phenotypes observed in *Trp53*$^{-/-}$ male (M) and female (F) mice result from p53 loss of function (LOF), whereas those observed in *Trp53*$^{Y217C/Y217C}$ mice result from p53 LOF as well as additional effects (gain of function (GOF) in red). The + signs denote the presence of a phenotype. Xi: X chromosome inactivation.

Locus	Forward Primer	Reverse Primer	Purpose
Trp53	GCGTAGTGGTACCTTGTGAGCCCCCCGAGGTCT	ACCTCGGGGGGCTCACAAGGTACCACTACGCTG	Mutagenesis (YC-F/R)
Trp53	CCTGGGAATACTTCAAGAGACG	CGTGATATTGCTGAAGAGCTTG	Genotyping (a, b)
Trp53	GTGTGTTGGCCATCTCTGTG	AACCGGACTCAGCGTCTCTA	Genotyping (c, d)
Ccl17	GCTGGTATAAGACCTCAGTGGAGTGT	GCTTGCCCTGGACAGTCAGA	qPCR
Ccl9	GCACAGCAAGGGCTTGAAA	CAGGCAGCAATCTGAAGAGTCTT	qPCR
Ccr3	CTGGACTCATAAAGGACTTAGCAAAA	TCTTGATTTCATCTGTGTTGAATGC	qPCR
Cdkn1a	GCAGACCAGCCTGACAGATTTC	TTCAGGGTTTTCTCTTGCAGAAG	qPCR
Cxcl10	AATGAAAGCGTTTAGCCAAAAAA	GGTGTGTGCGTGGCTTCAC	qPCR
Maob	GGTACAACCAGAATCATCTCAACAA	CTTGACCAGATCCACCAATAAATTT	qPCR
Mdm2	GTCTACCGAGGGTGCTGCAA	AAGCAATGGTTTTGGTCTAACCA	qPCR
Noxa	CCTGGGAAGTCGCAAAAGAG	GAGCACACTCGTCCTTCAAGTCT	qPCR
Pls3	CCAGCACTAACTAAACCTGAAAACC	GGTTCTTTCTTCCCGAGTTTCC	qPCR
S100a8	TCCTTTGTCAGCTCCGTCTTC	GACGGCATTGTCACGAAAGAT	qPCR
S100a9	ACAAATGGTGGAAGCACAGTTG	TCATTTATGAGGGCTTCATTTCTCT	qPCR
Trp53	AAAGGATGCCCATGCTACAGA	TCTTGGTCTTCAGGTAGCTGGAG	qPCR
Usp9x	CTTGCTCAGCAGATTTCTGATGA	GCTGTAATCCTCCACATCCTGAT	qPCR
Ppia	TCTCCTTCGAGCTGTTTGCA	CAGTGCTCAGAGCTCGAAAGTTT	qPCR (control)
Rplp-0	CGACCTGGAAGTCCAACTAC	ATCTGCTGCATCTGCTTG	qPCR (control)
Cdkn1a	GTGAGGAGGAGCATGAATGGA	GGCAAAGTGGGACGTCCTTA	ChIP
Mdm2	CCGAGTTGACTCAGCTCTTCCT	ACCCCAGCTGGAGACATGTC	ChIP
Rbl2	CCAAGGGAAGCCACATGGT	ACCAGCCTTTCCATCTGCAT	ChIP (control)

Table S8. Primers used in this study.